

# Loss of Zfp335 triggers cGAS/STING-dependent apoptosis of post- $\beta$ selection pre-T cells

Jeremy Ratiu (✉ [Jeremy.Ratiu@duke.edu](mailto:Jeremy.Ratiu@duke.edu))

Duke University School of Medicine <https://orcid.org/0000-0001-9234-7674>

William Barclay

Duke University

Qun Wang

Duke University

Sebastian Wellford

Duke University <https://orcid.org/0000-0002-2535-6893>

Naren Mehta

Duke University <https://orcid.org/0000-0003-0829-3592>

Melissa Harnois

Duke University <https://orcid.org/0000-0002-5910-6198>

Devon DiPalma

Duke University

Sumedha Roy

Duke University

Alejandra Contreras

Fox Chase Cancer Center

Mari Shinohara

Duke University School of Medicine <https://orcid.org/0000-0002-6808-9844>

David Wiest

Temple University Health System <https://orcid.org/0000-0002-0792-3188>

Yuan Zhuang

Duke University Medical Center

---

## Article

## Keywords:

**Posted Date:** January 25th, 2022

**DOI:** <https://doi.org/10.21203/rs.3.rs-1226201/v1>

**License:**  This work is licensed under a Creative Commons Attribution 4.0 International License.

[Read Full License](#)

---

**Version of Record:** A version of this preprint was published at Nature Communications on October 6th, 2022. See the published version at <https://doi.org/10.1038/s41467-022-33610-4>.

1 **Loss of Zfp335 triggers cGAS/STING-dependent apoptosis of post- $\beta$  selection**  
2 **pre-T cells**

3 Jeremy J Ratiu<sup>1\*</sup>, William E Barclay<sup>1</sup>, Qun Wang<sup>1</sup>, Sebastian Wellford<sup>1</sup>, Naren Mehta<sup>1</sup>,  
4 Melissa J Harnois<sup>1</sup>, Devon DiPalma<sup>1</sup>, Sumedha Roy<sup>1</sup>, Alejandra V Contreras<sup>2</sup>, Mari L  
5 Shinohara<sup>1,3</sup>, David Wiest<sup>2</sup>, Yuan Zhuang<sup>1</sup>

6 <sup>1</sup> Duke University, Department of Immunology, Durham, NC 27710

7 <sup>2</sup> Fox Chase Cancer Center, Blood Cell Development and Function Program,  
8 Philadelphia, PA 19111

9 <sup>3</sup> Duke University, Department of Molecular Genetics and Microbiology, Durham, NC  
10 27710

11 \* Correspondence: Jeremy.Ratiu@duke.edu

12

13 **Abstract**

14 Production of a diverse peripheral T cell compartment requires massive  
15 expansion of the bone marrow progenitors that seed the thymus. There are two main  
16 phases of expansion during T cell development, following T lineage commitment at the  
17 DN2 stage and following successful rearrangement and selection for functional TCR $\beta$   
18 chains in DN3 thymocytes, which promotes development of DN4 cells to the DP stage.  
19 Signals driving expansion of DN2 thymocytes are well studied, however, factors  
20 regulating the proliferation and survival of DN4 cells remain poorly understood. Here,  
21 we uncover an unexpected link between the transcription factor Zfp335 and control of  
22 cGAS/STING-dependent cell death in post- $\beta$ -selection DN4 thymocytes. Zfp335 controls

23 survival by sustaining expression of Ankle2, which suppresses cGAS/STING-dependent  
24 cell death. Together, this study identifies Zfp335 as a key transcription factor controlling  
25 the survival of proliferating post- $\beta$ -selection thymocytes and demonstrates a key role for  
26 the cGAS/STING pathway driving apoptosis of developing T cells.

## 27 **Introduction**

28 Development of large number of T cells with clonally acquired T cell receptor  
29 (TCR) in the thymus demands a small number of bone marrow derived progenitors to  
30 undergo vigorous expansion prior to each of the sequentially ordered TCR gene  
31 rearrangement events. The first major expansion occurs immediately upon T lineage  
32 commitment at the DN2 stage prior to rearrangement of any TCR gene<sup>1, 2, 3, 4</sup>. The  
33 expanded T cell progenitors enter the DN3 stage where rearrangement at the TCR $\beta$ ,  $\gamma$ ,  
34  $\delta$  gene loci become permissive. In postnatal thymus, the majority of DN3 cells will  
35 choose the  $\alpha\beta$ T cell fate due to the generation of a productively rearranged TCR $\beta$  chain.  
36 Post  $\beta$ -selection DN3 cells then move to the DN4 stage where the second phase of  
37 expansion occurs, typically involving several rounds of rapid proliferation over the  
38 course of 2-3 days in mice. The expansion of TCR $\beta$  positive cells result in generation of  
39 the post mitotic DP cells, which constitutes 90% of all thymocytes in post-natal mice and  
40 humans. DP cells undergo TCR $\alpha$  gene rearrangement and selection, a process  
41 resulting in approximately 1% of cells surviving and contributing to the peripheral T cell  
42 pool. Therefore, the expansion of post  $\beta$ -selection DN4 cells prior to TCR $\alpha$  gene  
43 rearrangement and TCR selection represents a critical amplifier to control the output of  
44  $\alpha\beta$ T cells from the thymus.

45 While most stages of T cell development have been subject to extensive genetic  
46 and functional characterization, the post- $\beta$ -selection proliferative phase remains less  
47 well understood. Previous studies have shown that proliferation but not survival of DN4  
48 cells is dependent upon IL-7R signaling which functions to repress Bcl6 expression<sup>5</sup>.  
49 Similarly, proliferation during this stage of development also requires the combined  
50 activities of NOTCH and pre-TCR signaling<sup>6, 7, 8, 9</sup>. This effect is in part the result of  
51 induction of Fbxl1 and Fbxl12 which induce polyubiquitination and proteasomal  
52 degradation of Cdkn1b ensuring proper cell cycle progression and proliferation<sup>10</sup>.  
53 Survival of proliferating post- $\beta$ -selection thymocytes was found to require expression of  
54 the chromatin associated protein yin yang 1 (Yy1), the absence of which drives p53-  
55 dependent apoptosis<sup>11</sup>. Animal models exploring cell death during T cell development  
56 have repeatedly shown thymocyte apoptosis, including among DN4 cells, is largely  
57 driven by activities of pro-apoptotic Bcl2 family proteins<sup>12, 13, 14, 15, 16</sup>. Pathways  
58 controlling the survival and death of early proliferating thymocytes upstream of the Bcl2  
59 family remain largely unexplored.

60 Underpinning the fate decisions of thymocytes are vast transcriptional networks  
61 which coordinate the intricate changes and checkpoint traversals required for proper  
62 development<sup>17</sup>. Numerous transcription factors function at different stages to achieve  
63 this result. One transcription factors family of particular importance are the basic helix-  
64 loop-helix E proteins, which include E2A, HEB and E2-2. In developing T cells, activities  
65 of the E2A and HEB have been shown to regulate nearly all stages of thymopoiesis<sup>18</sup>.  
66<sup>19</sup>. These E proteins play critical roles in enforcing the  $\beta$ -selection checkpoint by  
67 promoting expression of *Rag1/2*<sup>20</sup> and *pre-Ta*<sup>21</sup>, activation of the TCR $\beta$ <sup>22</sup>, TCR $\gamma$ , and

68 TCR $\delta$  loci <sup>23</sup> and preventing passage of DN cells lacking a functional TCR $\beta$  chain from  
69 progressing to the DP stage <sup>24, 25</sup>. Additionally, E protein activity has been shown to  
70 enforce early T cell lineage commitment <sup>26</sup> and promote survival of post- $\beta$ -selection DP  
71 thymocytes undergoing TCR $\alpha$  recombination <sup>27</sup>. Together, the combined activities of E  
72 proteins play critical and indispensable roles in the establishment of a functional T cell  
73 repertoire. However, due to the widespread binding of these factors throughout the  
74 genome of developing thymocytes our understanding of their roles in development are  
75 far from complete.

76         The cGAS/STING pathway functions to sense cytosolic DNA and initiate innate  
77 immune responses <sup>28</sup>. Cyclic GMP-AMP (cGAMP) synthase (cGAS) recognizes dsDNA,  
78 typically of foreign origin, catalyzing the generation of the cyclic dinucleotide (CDN)  
79 second messenger cGAMP which in turn drives STING activation and down-stream  
80 signaling <sup>29</sup>. The cGAS/STING pathway is best known for its functions in non-immune  
81 and innate immune cells such as macrophage and dendritic cells in the context of viral  
82 or bacterial infections. In these contexts, activation of the pathway typically results in the  
83 production of type I interferons and other pro-inflammatory mediators. Recent work has  
84 shown that the cGAS/STING pathway is also highly active but functionally divergent  
85 within T cells, primarily driving type I interferon-independent responses and apoptosis <sup>30,</sup>  
86 <sup>31, 32, 33</sup>. Under steady-state conditions the cGAS/STING pathway plays a minimal role in  
87 T cell development as evidenced by normal thymic T cell subset proportions and overall  
88 thymus size in cGAS or STING-deficient C57/BL6 mice <sup>32</sup>. However, it remains to be  
89 determined whether the cGAS/STING pathway plays a role in sensing and responding  
90 to cell intrinsic stresses during thymic T cell development.

91 In this study we show that loss of Zinc finger transcription factor 335 (Zfp335),  
92 triggered cGAS/STING-mediated apoptosis among proliferating DN4 cells. Zfp335 was  
93 initially identified from genetic mapping of familial traits that cause a severe form of  
94 microcephaly<sup>34</sup>. Using a conditional knockout mouse model<sup>34, 35</sup> we show that loss of  
95 Zfp335 promotes cGAS/STING dependent apoptosis among proliferating post- $\beta$ -  
96 selection DN4 thymocytes, severe reduction in overall thymic cellularity and a near  
97 absence of peripheral T cells. Mechanistically, Zfp335 functions to suppress  
98 cGAS/STING activation through promoting Ankle2 expression which in turn regulates  
99 the cGAS inhibitor Baf<sup>36</sup>. The importance of cGAS/STING pathway among DN4  
100 thymocytes was further demonstrated by their sensitivity to STING agonist and STING-  
101 mediated cell death in wild type mice. Thus, we have uncovered for the first time a role  
102 for the cGAS/STING pathway in regulating thymic T cell development and identify the  
103 Zfp335/Ankle2/Baf axis as the first transcriptional network functioning to regulate  
104 cGAS/STING activity.

105

## 106 **Results**

### 107 Zfp335, an E-protein target, is critical for T cell development

108 The E protein family of transcription factors are indispensable regulators of nearly  
109 every stage of T cell development<sup>4, 17, 22, 24, 27, 37, 38, 39, 40</sup>. E proteins control complex  
110 transcriptional networks which remain incompletely understood. To gain deeper insight  
111 into mechanisms by which E proteins regulate T cell development, we previously  
112 performed E2A ChIP-seq to identify the genome-wide binding sites during T cell

113 development<sup>40</sup>. We identified *Zfp335* as an E protein target during T cell development  
114 (Fig S1A). Analysis of published data showed E protein-deficient thymocytes exhibit  
115 significantly reduced *Zfp335* expression (Fig S1B)<sup>39</sup>. Since germline deletion of *Zfp335*  
116 is non-viable<sup>34</sup> we utilized a conditional deletion model driven in which Cre expression is  
117 controlled by the E8<sub>III</sub> enhancer of *Cd8a* (E8<sub>III</sub>-cre) to allow functional assessment of  
118 *Zfp335* in post- $\beta$ -selection thymocytes<sup>35</sup>. There are conflicting reports regarding the  
119 deletion kinetics for this Cre<sup>35, 41</sup>, therefore, we began by assessing its activity across T  
120 cell development in our system (Fig S1C-D). Consistent with Dashtsoodol *et al.*, we  
121 found E8<sub>III</sub>-cre is highly active immediately upon entry into DN3a with no recombination  
122 activity evident in the preceding DN2 stage. However, recombination does not appear to  
123 be complete until the DP stage.

124 We subsequently assessed *Zfp335*<sup>fl/fl</sup> E8<sub>III</sub>-cre (*Zfp335*cKO) mice for thymic T cell  
125 development. Deletion of *Zfp335* led to a significant reduction in total thymic cellularity  
126 (Fig 1A-B). This reduction in thymic cellularity is likely due to defects in the  $\alpha\beta$  lineage  
127 as numbers of  $\gamma\delta$  T cells were not altered (Fig 1C-D). Assessment of developmental  
128 stages revealed the reduction in thymocyte numbers of *Zfp335*cKO mice begins at the  
129 DN4 stage (Fig 1E-I).

130 Examination of the peripheral T cell compartment revealed significantly reduced  
131 numbers of splenic T cells in *Zfp335*cKO mice (Fig S2A-K). A previous study identified  
132 the hypomorphic *Zfp335*<sup>bloto</sup> allele as the causative mutation in a unique form of T  
133 lymphopenia<sup>42</sup>. Like *Zfp335*<sup>bloto</sup> mice, we found that peripheral T cells in *Zfp335*cKO  
134 mice were almost exclusively of an effector or memory phenotype suggesting these  
135 mice also exhibit a similar defect in the establishment of the naïve T cell compartment.

136 To determine the transcriptional changes resulting from loss of Zfp335 we  
137 performed RNA-seq on Zfp335cKO DP thymocytes. DP cells were used as they were  
138 the first population exhibiting complete deletion (Fig S1D). We found that loss of Zfp335  
139 results in differential expression of 327 genes (113 down, 214 up; Fig 1K,J). Among the  
140 161 Zfp335 ChIP-seq targets identified in thymocytes<sup>42</sup>, 34 were down-regulated in  
141 Zfp335cKO mice (Fig 1K). No Zfp335 target genes were up-regulated in Zfp335cKO  
142 samples (Fig 1K) corroborating previous findings that Zfp335 primarily functions as a  
143 transcriptional activator<sup>34, 42</sup>. Consistent with transcriptomic analyses of *Zfp335<sup>bloto</sup>*  
144 mice<sup>42</sup>, gene set enrichment analysis (GSEA) revealed significant enrichment among  
145 type I and type III interferon signaling and P53 signaling pathways in Zfp335cKO DP  
146 cells (Fig 1L). Together, these findings identify Zfp335 as a key transcription factor  
147 regulating T cell development.

#### 148 Loss of Zfp335 in DN3 thymocytes does not impair $\beta$ -selection

149 Zfp335 deletion results in reduced cell numbers beginning at the DN4 stage,  
150 raising the possibility that the inability to rearrange the TCR $\beta$  locus could be  
151 responsible. Consequently, we assessed TCR $\beta$  rearrangement in DN3 and DN4  
152 thymocytes by intracellular staining. The frequency of icTCR $\beta$ <sup>+</sup> cells among Zfp335cKO  
153 DN3 and DN4 subsets was comparable to that of WT (Fig S3A-C). Therefore, TCR $\beta$   
154 rearrangement and subsequent pre-TCR expression are unimpaired in Zfp335cKO  
155 mice.

156 In addition to pre-TCR expression, to successfully traverse the  $\beta$ -selection  
157 checkpoint, pre-TCR signals are required for release from cell cycle arrest, survival and  
158 progression to DP<sup>43</sup>. CD27 surface expression is increased by pre-TCR signals in DN3

159 thymocytes<sup>44</sup>. Zfp335cKO DN3 thymocytes exhibited CD27 upregulation comparable to  
160 that of WT (Fig S3D-E) indicating Zfp335-deficiency does not lead to impaired pre-TCR  
161 signaling. Together, these results indicate that the observed reduction of DN4 cells in  
162 Zfp335cKO mice did not result from failure to produce TCR $\beta$  subunits or failure to  
163 transduce pre-TCR signals.

164

#### 165 Zfp335 inhibits apoptosis during the DN-DP transition

166 Zfp335 deletion during the DN3 stage leads to severe defects in T cell  
167 development, likely during the post- $\beta$ -selection proliferative phase. To determine if  
168 Zfp335-deficiency altered either the proliferation or survival of post- $\beta$ -selection  
169 thymocytes, we directly measured these events in OP9-DL1 cultures *in vitro*<sup>45</sup>.  
170 Consistent with our *ex vivo* data, Zfp335cKO cells exhibit severely impaired progression  
171 to the DP stage (Fig 2A-B). Zfp335cKO cells exhibited modestly reduced proliferation  
172 compared to controls (Fig 2C-D). In contrast, Zfp335cKO cells underwent substantially  
173 increased rates of apoptosis (Fig 2E-F). Importantly, proliferation tracking (Fig 2G) and  
174 assessment of developmental progression (Fig 2H) of apoptotic mutant cells  
175 demonstrate they have undergone cell division and largely remain DN. These data  
176 suggest that Zfp335cKO cells are dying during the post- $\beta$ -selection proliferative phase  
177 and that Zfp335 activity promotes the survival of DN4 thymocytes.

178

#### 179 Ectopic Bcl2 expression rescues the developmental defect resulting from loss of Zfp335

180 Our RNA-seq studies revealed Zfp335cKO thymocytes exhibit increased  
181 expression of the pro-apoptotic Bcl2-family members, PUMA (*Bbc3*), NOXA (*Pmaip1*)  
182 and *Bax* (Fig 3A), suggesting that these factors may be responsible for the observed  
183 increase in apoptosis among Zfp335cKO thymocytes. The function of these proteins  
184 can be antagonized by ectopic expression Bcl2. Thus, we asked whether Bcl2  
185 overexpression could rescue Zfp335cKO thymocyte apoptosis. WT or Zfp335cKO  
186 DN3/4 thymocytes were transduced with control or Bcl2-expressing retroviruses then  
187 grown in the OP9-DL1 culture system. Bcl2 overexpression significantly reduced  
188 apoptosis in Zfp335cKO cells, indicating the induction of pro-apoptotic Bcl2 family  
189 members was at least partially responsible for the observed increase in apoptosis in  
190 Zfp335-deficient thymocytes (Fig 3B-C).

191 We next sought to test the ability of Bcl2 overexpression to rescue Zfp335-  
192 deficient cells from apoptosis *in vivo* through generating Bcl2 conditional transgenic  
193 mice (Fig 3D). Intracellular staining revealed that *Zfp335<sup>fl/fl</sup> R26<sup>LSL-Bcl2-Tg</sup> E8<sup>III-cre</sup>*  
194 (Zfp335cKO Bcl2-Tg) thymocytes exhibited increased Bcl2 protein expression relative to  
195 WT (Fig 4E). Phenotypic analysis demonstrated that ectopic Bcl2 expression was able  
196 to fully rescue the early developmental defects observed in Zfp335-deficient mice,  
197 restoring traversal of the  $\beta$ -selection checkpoint, transition to the DP stage, and total  
198 thymic cellularity (Fig 3F-L).

199 Consistent with studies of *Zfp335<sup>bloto</sup>* mice<sup>42</sup>, Bcl2 overexpression failed to rescue  
200 the impairment in final single positive thymocyte maturation (Fig S4A-C) or peripheral T  
201 cell compartment numbers (Fig S4D-E) and effector status (Fig S4F-H). Taken together,  
202 these data suggest that the early impairment of thymocyte development following loss

203 of Zfp335 expression is due to increased rates of DN4 apoptosis driven by pro-apoptotic  
204 Bcl2-family members. However, our *in vivo* studies also revealed an additional, Bcl2-  
205 independent late block in terminal T cell differentiation within the thymus.

206

#### 207 Defining the ‘true’ DN4 thymocyte population at the single cell level

208 The DN4 stage of T cell development remains poorly understood and, as a  
209 result, poorly defined. DN4 cells are identified by lack of expression of identifying  
210 markers associated with any other thymocyte subset. Based on these criteria, it is  
211 possible that DN4 cells defined by marker exclusion may not be homogenous. To  
212 assess whether there is any heterogeneity in the DN4 compartment exacerbated by  
213 Zfp335-deficiency, we performed scRNA-seq of phenotypically defined DN4 cells. After  
214 quality control, libraries yielded transcriptome data for 6,537 or 5,392 high-quality cells  
215 from WT or Zfp335cKO samples, respectively.

216 We identified 10 unique cell clusters (Fig 4A-C). Five clusters were largely  
217 cycling cells (DN4\_1-5; Fig 4A-B) uniquely expressing *Ptcra* (pre-T $\alpha$ ) and proliferation  
218 associated genes (*Mki67*, *Cdk1*) (Fig 4D), representing bona fide DN4 cells. Three  
219 clusters (Mat\_1-3) expressed high levels of *Trac* and *Trbc1* transcripts (Fig 4D). Two  
220 additional clusters (gd17 and gd1) of  $\gamma\delta$  T cells were identified. gd17 cells express high  
221 levels of *Sox13*, *Rorc* and *Maf*, features of  $\gamma\delta$ 17 while gd1 express *Nkg7*, *Il2rb*, *S1pr1*  
222 and *Il7r* associated with cytotoxic  $\gamma\delta$  T cells (Fig 4D). Based on this clustering, Zfp335-  
223 deficiency led to substantial proportional increases and decreases in the  $\gamma\delta$  T cell  
224 clusters and Mat\_2 cluster relative to WT control, respectively (Fig 4C).

225 We were surprised to find a large proportion of phenotypically defined DN4  
226 thymocytes expressing *Trac* transcripts and sought to define these populations.  
227 Consistent with their lack of surface CD4 or CD8 these cells uniformly lacked *Cd4*,  
228 *Cd8a* and *Cd8b1* transcripts (Fig 4D). We hypothesized that these cells may represent  
229 post-positive selection thymocytes that transiently down-regulated surface TCR, CD4  
230 and CD8 expression. Consistent with our hypothesis, we found these cells express high  
231 levels of *Nr4a1*, *Cd69*, *Pdcd1*, *Egr1*, *Cd2*, and *Itm2a*, signature genes of positive  
232 selection <sup>46</sup>. Based on this profile we define cells from these clusters as maturing  $\alpha\beta$  T  
233 cells.

234 Importantly, most cells associated with the maturing  $\alpha\beta$  or  $\gamma\delta$  T cell clusters were  
235 non-cycling (Fig 4B), and therefore, not 'true' DN4 cells. Retroviral transduction  
236 depends on cell being cycling<sup>47</sup>. Therefore, we determined whether 'true' DN4 cells  
237 could be separated from contaminating populations *ex vivo* with retroviruses. Virally  
238 transduced or non-transduced DN4 cells were placed in OP9-DL1 culture. Non-  
239 transduced DN4 cells preferentially give rise to single-positive cells expressing high  
240 levels of surface TCR, whereas, transduced DN4 become DP (Fig 4F-G). Since OP9-  
241 DL1 cells are unable to support positive selection, we conclude that these non-  
242 transduced DN4 cells are post-positive selection cells transitioning to SP. Together,  
243 these results demonstrate that the phenotypically defined DN4 compartment is  
244 heterogenous and establishes retroviral transduction as a method to isolate DN4 cells  
245 for *in vitro* analysis.

246

247 [Ankle2 is a critical Zfp335-regulated gene required for survival of DN4 thymocytes](#)

248           Next, we focused our scRNA-seq analyses on determining the transcriptional  
249 changes in DN4 cells resulting from loss of *Zfp335*. Maturing  $\alpha\beta$  and  $\gamma\delta$  cells were  
250 removed leaving only ‘true’ DN4 cells. Based on recombination kinetics (Fig S1D) not all  
251 *Zfp335*cKO DN4 cells have undergone deletion. *Zfp335* expression could not reliably  
252 delineate mutant from non-mutant cells due to low detection rate (8% of *Zfp335*cKO vs  
253 17.7% of WT cells). To identify true mutant DN4 cells in our dataset, we assessed  
254 transcription factor activity using gene set scores calculated for each cell based on the  
255 expression of the *Zfp335* ChIP-seq target genes down-regulated in mutant DP cells (Fig  
256 1J,K). *Zfp335*cKO cells exhibited a bimodal distribution for the gene set. Using  
257 established methods<sup>48</sup>, cutoff values were determined for the distribution and cells  
258 falling below this threshold were considered true mutants (Fig S5A). Cutoffs were  
259 confirmed by differential expression analysis between WT and *Zfp335*cKO targets high  
260 or *Zfp335*cKO targets low cells. Compared to WT, *Zfp335*cKO targets low cells  
261 exhibited differential expression of 80 genes (60 down, 20 up; Fig S4B) whereas  
262 *Zfp335*cKO targets high cells only exhibited differential expression of 7 genes (5 down,  
263 2 up; Fig S4C).

264           *Zfp335*cKO cells above the threshold were considered non-mutant, removed and  
265 the remaining cells were then reanalyzed (Fig 5A) identifying 8 unique clusters (Fig  
266 S4D). WT and mutant cells were distributed across each cluster. C1-3 were enriched for  
267 WT whereas C4 was almost entirely mutant cells (Fig S4E). Despite regression of  
268 standard cell cycle-associated genes, clustering was largely dictated by cell cycle (Fig  
269 S4F-I). We observed no differences in cell cycle phase distributions between WT and  
270 mutant (Fig S4H). Therefore, we chose to compare WT and mutant DN4 cells based on

271 genotype. Among the 60 down-regulated genes in mutant DN4 cells, 44 are Zfp335  
272 targets by ChIP-seq (Fig 5B)<sup>42</sup>. We hypothesized that reduced expression of one or  
273 more of these genes was responsible for the increased rates of apoptosis observed in  
274 mutant DN4 cells. Thus, we examined expression of the 12 Zfp335 target genes with  
275 experimental evidence demonstrating a negative regulatory role in cell death (Fig 5C-  
276 D). Four exhibited reduced expression in mutant DN4 thymocytes (Fig 5C). Examination  
277 of expression frequency identified *Ankle2* to have the greatest reduction in percent of  
278 mutant cells expression (Fig 5E).

279 *Ankle2* encodes an ER-restricted ankyrin repeat and LEM domain-containing  
280 protein<sup>49</sup>. *Ankle2* was recently identified as a critical Zfp335-regulated factor in the  
281 establishment of the naïve T cell<sup>42</sup>. Therefore, we tested whether *Ankle2*  
282 overexpression could rescue Zfp335cKO apoptosis. WT or Zfp335cKO DN3 thymocytes  
283 were transduced with EV or Ankle2 retrovirus and cultured on OP9-DL1 cells.  
284 Importantly, *Ankle2* overexpression was able to fully rescue Zfp335-deficient  
285 thymocytes from increased rates of apoptosis (Fig 5F-G). Moreover, *Ankle2*  
286 overexpression led to significantly increased proportions of DP cells among Zfp335cKO  
287 samples (Fig 5H).

288 Next, we sought to confirm that *Ankle2* expression is directly regulated by Zfp335  
289 in pre-T cells. Analysis of published ChIP-seq data showed Zfp335 binds the proximal  
290 promoter of *Ankle2* in thymocytes (Fig 5I). To examine the relationship between *Zfp335*  
291 and *Ankle2* expression we utilize the DN4-like mouse thymocyte cell line *Scid.adh.2c2*<sup>60</sup>  
292 for CRISPR-based transcriptional inhibition (CRISPRi) studies<sup>51</sup>. These cells were  
293 transduced with retroviruses expressing *Zfp335* promoter-targeting gRNA and anti-

294 GCN4scFv-sfGFP-KRAB fusion construct. *Zfp335*-targeted cells exhibited reduced  
295 *Ankle2* expression proportional to the efficiency of *Zfp335* knock-down (KD) (Fig 5J).  
296 Additionally, *Zfp335*KD resulted in increased expression of *Bax* like that observed in  
297 *Zfp335*cKO thymocytes (Fig. 5K). Together, these results demonstrate a direct  
298 relationship between *Zfp335* and *Ankle2* expression in developing T cells and suggest  
299 reduced *Ankle2* expression resulting from loss of *Zfp335* drives DN4 apoptosis in  
300 *Zfp335*cKO mice.

301

302 Disruption of the *Zfp335*/*Ankle2*/*Baf* axis drives cGAS/STING-dependent apoptosis of  
303 DN4 thymocytes

304 Next, we sought to determine the mechanism driving this increase in cell death  
305 resulting from reduced *Ankle2* expression. *Ankle2* has previously been shown to control  
306 nuclear envelope (NE) reassembly and integrity following mitosis through regulation of  
307 Barrier to Autointegration Factor 1 (*Banf1* or *Baf*) phosphorylation. Consistent with  
308 reduced *Ankle2* expression we observed significant increases in *Baf* phosphorylation  
309 among *Zfp335*cKO DN4 thymocytes (Fig 6A-C). Additionally, as previously reported,  
310 disruption of *ANKLE2* or *BANF1* expression in Hela cells led to severe disruptions in NE  
311 architecture (Fig S6A). To determine if the same is true for *Zfp335*-deficient DN4  
312 thymocytes we examined the NE *ex vivo*. Indeed, *Zfp335*cKO DN4 thymocytes exhibit  
313 significantly altered NE architecture characterized by diffuse Lamin B1 throughout the  
314 cytosol, reduced DAPI signal possibly the result of loss of nuclear-cytosolic  
315 compartmentalization, and reduced nuclear sphericity (Fig 6D-G). Together, these data

316 confirm that loss of Zfp335 leads to significantly altered NE architecture consistent with  
317 dysregulation of Ankle2/Baf-mediated NE reassembly and maintenance.

318         Accumulation of cytosolic DNA or exposure of nuclear contents to the cytosol via  
319 NE disruption have been shown to activate the cGAS/STING pathway<sup>36, 52</sup>. In T cells,  
320 cGAS/STING signaling generally results in anti-proliferative and pro-apoptotic effects<sup>30,</sup>  
321 <sup>31, 33, 53</sup>. Therefore, we hypothesized that NE defects resulting from disruption of the  
322 Ankle2-Banf1 pathway downstream of Zfp335 loss drives cGAS/STING activation.  
323 Consistent with this hypothesis, GSEA revealed an enrichment for genes upregulated  
324 by T cells in response to STING signaling in both our bulk DP and single-cell DN4  
325 datasets (Fig 6H,I). Additionally, we found increased IRF3 activity among mutant cells  
326 (Fig 6J). cGAS/STING-mediated death of mature T cells occur in part, due to increased  
327 expression of pro-apoptotic Bcl2 family genes<sup>31</sup>. Like our findings from bulk RNA-seq  
328 (Fig 4A), we also observed increased expression of Bbc3 (PUMA), Pmaip1 (NOXA),  
329 Bcl2l11 (Bid) and Bax among Zfp335cKO DN4 cells in our scRNA-seq dataset (Fig 6K).

330         In addition to nuclear DNA, mitochondrial DNA (mtDNA) serves as a substrate for  
331 cGAS<sup>54</sup>. mtDNA release requires mitochondrial outer membrane permeabilization  
332 resulting in mitochondrial membrane depolarization<sup>55</sup>. Examination of mitochondria  
333 showed Zfp335cKO thymocytes exhibit normal mitochondrial membrane potential and  
334 total mitochondrial mass (Fig S6B-C). Therefore, mtDNA release is unlikely to be driving  
335 cGAS/STING-mediated death following loss of Zfp335. Instead, exposure of gDNA to  
336 cytosolic cGAS resulting from disrupted nuclear envelope architecture is the most likely  
337 cause.

338 To test the contribution of cGAS/STING to increased rates of DN4 apoptosis in  
339 Zfp335cKO mice 'true' DN4 cells were isolated by EV viral transduction then placed in  
340 OP9-DL1 culture for 3 days with cGAS (RU.521)<sup>56</sup> or STING (H-151)<sup>57</sup> inhibitors.  
341 Chemical inhibition of either cGAS or STING fully rescued Zfp335cKO DN4 cells from  
342 death (Fig 6L,M). Additionally, Zfp335cKO mice receiving H-151 for 7 days exhibited  
343 significantly increased numbers of total thymocytes compared to vehicle controls (Fig  
344 6N). Importantly, this increase in cellularity was primarily due to increased DP numbers  
345 (Fig 6O-R). Due to the short duration of treatment, we conclude that the increase in DP  
346 cells among H-151-treated Zfp335cKO mice is the result of reduced cell death during  
347 the preceding proliferative DN4 stage.

348 Next, we sought to determine the role of the Zfp335/Ankle2/Baf axis in  
349 suppressing the cGAS/STING-mediated apoptosis in DN4 cells. To test this, *R26<sup>LSL-Cas9</sup>*  
350 *Tcrd<sup>CreERT2</sup>* DN3/DN4 thymocytes<sup>58</sup> were transduced with retroviruses expressing  
351 *Zfp335*, *Ankle2*, or *Banf1* (encoding Baf) and *Mb21d1* (encoding cGAS) or *Tmem173*  
352 (encoding STING)-targeting gRNAs or non-targeting control gRNAs (NTG) then cultured  
353 for three days with OP9-DL1 cells in the presence of 4-hydroxytamoxifen. Consistent  
354 with conditional deletion, Cas9 targeting of *Zfp335* lead to a substantial increase in DN4  
355 apoptosis (Fig 6S). Additionally, targeting of *Ankle2* or *Banf1* similarly lead to increased  
356 DN4 apoptosis. Importantly, these increases in apoptosis were cGAS/STING-dependent  
357 (Fig 6S). Similar results were observed when Cas9 expression was controlled by E8<sub>III</sub>-  
358 cre (Fig S6D-E). Together, these results demonstrate that disruption of the  
359 Zfp335/Ankle2/Baf axis drives cGAS/STING-mediated apoptosis of post- $\beta$ -selection  
360 DN4 thymocytes.

361

362 DN4 thymocytes are uniquely sensitive to cGAS/STING-mediated cell death

363 Finally, we sought to determine whether sensitivity to cGAS/STING-driven cell  
364 death is a unique feature of Zfp335cKO DN4 cells or a mechanism of the DN4 stage.  
365 DN-enriched WT thymocytes were treated with the STING agonist cridanimod (CMA)  
366 overnight then assayed for apoptosis. Interestingly, we found DN4 cells are uniquely  
367 sensitive to STING-mediated apoptosis (Fig 6T-U). Additionally, viability of Zfp335cKO  
368 Bcl2-Tg thymocytes was not impacted by CMA treatment (Fig 6V) suggesting that  
369 induction of pro-apoptotic Bcl2 family members downstream of STING activation are  
370 necessary for apoptosis of DN4 thymocytes.

371 Together, these data demonstrate that activation of the cGAS/STING pathway is  
372 a major contributor to Zfp335cKO DN4 apoptosis and that WT DN4 cells are uniquely  
373 sensitive to cGAS/STING-mediated death. Altogether, our studies demonstrate that loss  
374 of Zfp335 leads to defective T cell development resulting from dysregulation of the  
375 Zfp335/Ankle2/Baf axis ultimately driving cGAS/STING-mediated DN4 cell death.

376

377 **Discussion**

378 In this study, we identify Zfp335 as a critical transcription factor regulating early T  
379 cell development within the thymus. Specifically, it functions to promote survival of  
380 proliferating cells following  $\beta$ -selection. Conditional deletion of Zfp335 led to severe  
381 reductions in all T cell populations beginning at the DN4 stage of development.  
382 Mechanistically, we show that reduced expression of the Zfp335-regulated gene Ankle2  
383 is responsible for increased sensitivity to cell death and disruption of the

384 Zfp335/Ankle2/Baf pathway controlling NE architecture drives cGAS/STING-dependent  
385 DN4 apoptosis.

386 Our studies provide the first comprehensive assessment of the heterogeneity  
387 within the DN4 thymocyte compartment at the single cell level. Surprisingly,  
388 phenotypically defined DN4 cells consist of cycling cells expressing pre-T $\alpha$  which  
389 represent 'true' DN4 cells and mature or maturing  $\alpha\beta$  and  $\gamma\delta$  T cells. Positive selection  
390 of DP thymocytes induces a slight, transient down-regulation of CD4 and CD8<sup>59</sup>,  
391 however, the maturing  $\alpha\beta$  cells identified in our dataset completely lack both protein and  
392 mRNA expression. The cells we identified expressing TCR $\alpha$  transcripts exhibited  
393 expression patterns consistent with positive selection<sup>46</sup> and therefore, are likely post  
394 positive-selection cells which have transiently lost surface expression of TCR, CD4 and  
395 CD8. Alternatively, these cells may have undergone positive selection without ever  
396 expressing CD4 or CD8. Regardless, these maturing cells may represent a novel  
397 developmental path within the thymus. However, more detailed studies will be needed  
398 to fully characterize these cells and determine if they represent a unique lineage or  
399 simply a rare differentiation path that can be taken by any positively selected cell.

400 Han *et al.* recently identified a hypomorph allele of *Zfp335* (*Zfp335<sup>bloto</sup>*) as the  
401 causative mutation leading to reduced total peripheral T cells and an almost complete  
402 absence of naïve T cells<sup>42</sup>. They found Ankle2 to be a critical *Zfp335*-regulated gene  
403 controlling late stages of thymic T cell maturation. However, the mechanism by which  
404 Ankle2 regulates maturation, and the establishment of the naïve T cell compartment  
405 remains unclear. The lack of apparent developmental defects in *Zfp335<sup>blt/blt</sup>* mice during  
406 early T cell development is likely due to their use of a hypomorph allele instead of a

407 conditional knock out as *Zfp335<sup>blt/blt</sup>* mice exhibited normal expression of Ankle2 during  
408 the DN4 stage.

409 We have shown that Zfp335 is at least partially regulated by E protein activity in  
410 developing T cells. E proteins play numerous indispensable roles throughout organismal  
411 development, including T cell development<sup>4, 22, 37, 38, 39, 40, 60, 61, 62</sup>. However, due to  
412 widespread binding throughout the genome, the roles for transcriptional networks  
413 established by E proteins remain incompletely understood<sup>40</sup>. Our studies identify Zfp335  
414 as a novel transcription factor downstream of E proteins critical to T cell development.

415 To date, studies of T cell-intrinsic roles for cGAS/STING pathway have largely  
416 focused on activation via synthetic STING agonists<sup>31, 33, 53</sup> or expression of constitutive  
417 gain-of-function STING mutations<sup>30</sup>. These studies have primarily focused on roles of  
418 this pathway in mature peripheral T cells. To our knowledge, this is the first report of a  
419 physiological role for cGAS/STING in T cell development. Additionally, our identification  
420 of the Zfp335/Ankle2/Baf axis as key in repression of cGAS is the first transcriptional  
421 pathway identified which functions to prevent cGAS activation by self-DNA.

422 Baf was recently identified as a key inhibitor of cGAS sensing of self-DNA  
423 through competitive binding<sup>36</sup>. The ability of Baf to bind DNA is dependent upon its  
424 dephosphorylation which has been shown to be controlled by Ankle2 during mitotic  
425 exit<sup>49</sup>. Therefore, we propose the following mechanism by which loss of Zfp335 drives  
426 cGAS/STING-mediated apoptosis of DN4 thymocytes. Loss of Zfp335 results in  
427 impaired Ankle2 expression which in turn leads to the failure of Baf dephosphorylation  
428 during division. Baf hyperphosphorylation leads to improper NE reassembly and can

429 drive spontaneous NE rupture exposing nuclear DNA to the cytosol allowing  
430 unrestricted cGAS activation and STING-mediated apoptosis.

431 Interestingly, in humans, ANKLE2 is a target of Zika virus protein NS4A which  
432 antagonizes its activity ultimately leading to microcephaly<sup>63</sup>. Humans carrying  
433 homozygous or compound heterozygous mutations in either ZNF335 or ANKLE2 exhibit  
434 severe microcephaly like that characteristic of Zika patients<sup>34, 64</sup>. Recent studies have  
435 demonstrated a critical role for central nervous system immune cells in regulating  
436 neuronal stem cell maintenance and differentiation. Specifically, microglia play a key  
437 role in this process<sup>65, 66, 67</sup>. Under conditions which stimulate cGAS activity, microglia  
438 and other CNS immune cells preferentially undergo apoptosis<sup>68</sup>. Based on the  
439 mechanism revealed in this study it is possible that microcephaly resulting from Zika  
440 infection or loss of ZNF335 or ANKLE2 may be driven by cGAS/STING-dependent  
441 apoptosis of neuronal progenitors and/ or CNS immune cells. Should our mechanism  
442 extend to neuronal progenitors or CNS immune cells it may be possible to  
443 pharmaceutically prevent microcephaly in these specific instances by inhibition of the  
444 cGAS/STING pathway. However, further research will be required to determine the  
445 viability of such a therapeutic approach.

#### 446 **Acknowledgements**

447 This study was funded by the NIH (R01-GM059638 and P01-AI102853) to YZ, (P01-  
448 AI102853) to DW, and (RO1-AI099100, RO1-NS120417, and RO1-AI160737) to MLS.

449 We thank M. Cook, N. Martin, B. Li and L. Martinek (Duke University Cancer Institute  
450 Flow Cytometry Core) for technical support and cell sorting. We thank the Duke

451 Molecular Physiology Institute for preparation of scRNA-seq libraries. We thank M.  
452 Krangel, QJ Li, J. Racine, D. Serreze, and M. Hasham for critical reading and  
453 comments on the manuscript. We thank M. Ciofani and J. Park for providing cell lines  
454 and mice. We thank M. Parker and J. Wheaton of M. Ciofani's lab for providing MSCV-  
455 Thy1.1 and MSCV-sgRNA expression vectors.

#### 456 **Author Contributions**

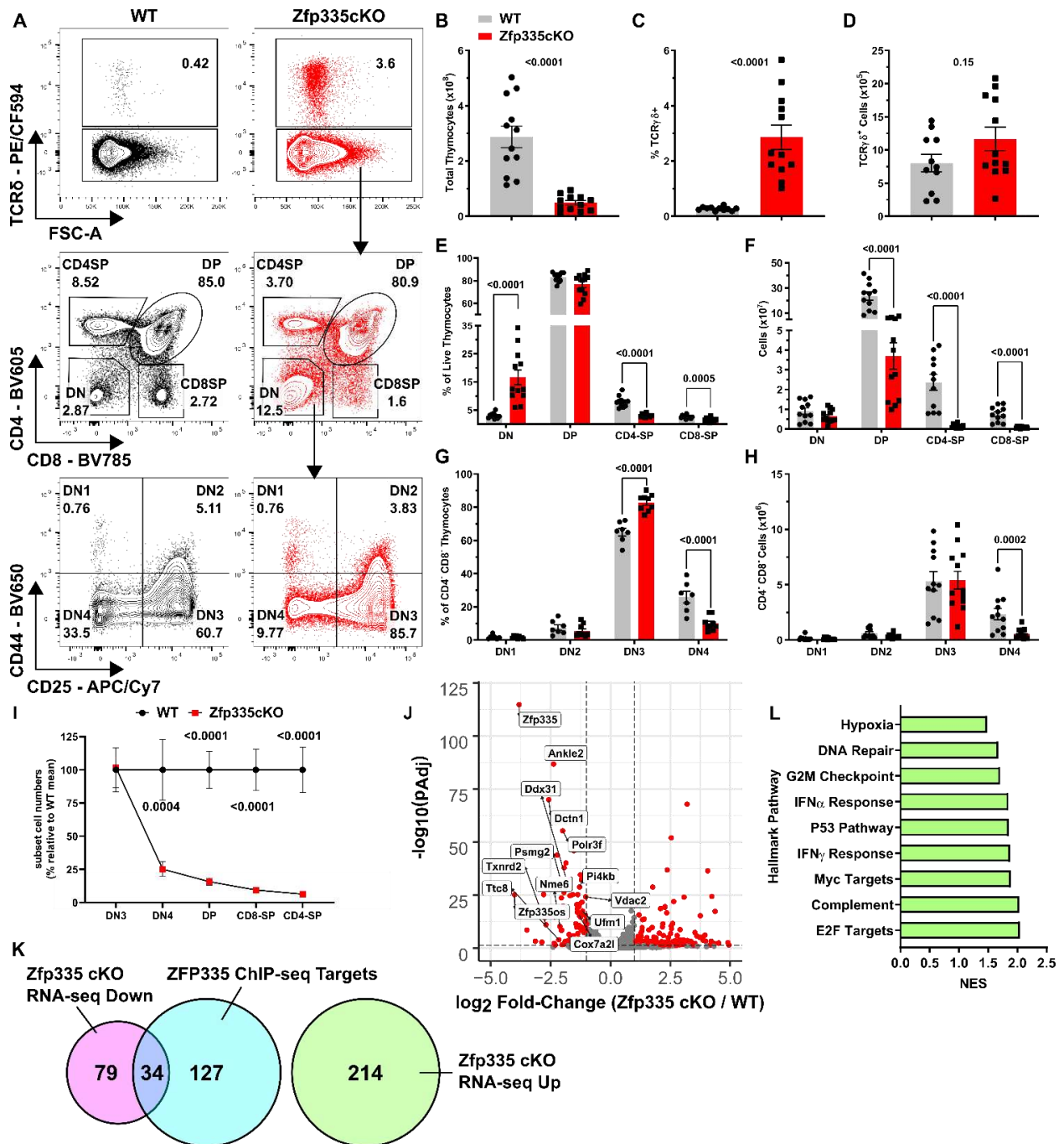
457 JJR, MLS, DW and YZ designed experiments and analyzed and interpreted data. JJR,  
458 WEB, QW, NM, DD, MJH, SW, SR and AVC performed experiments and analyzed data.  
459 JJR, YZ and DW wrote the manuscript with editing by the co-authors. JJR and YZ  
460 oversaw and supervised all aspects of the study.

#### 461 **Declaration of interests**

462 The authors declare no competing interests.

463

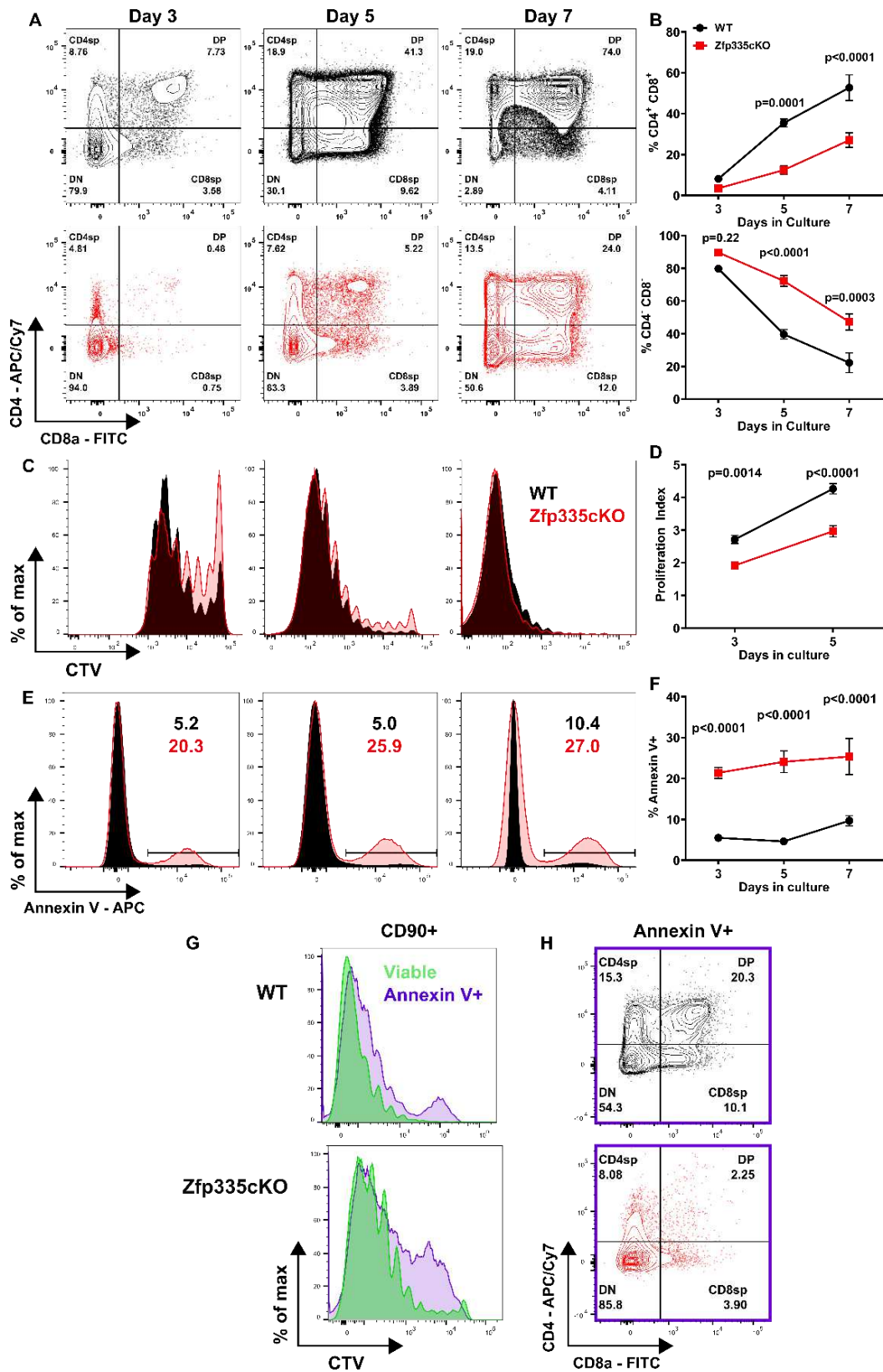
#### 464 **Figures**



465

466 **Figure 1 – Zfp335 is critical to  $\alpha\beta$  T cell development.** (A) Gating schema for *ex vivo* analysis  
 467 thymocyte development beginning with live thymocytes (DAPI $^-$  CD90.2 $^+$ , gating not shown). (B)  
 468 Total thymic cellularity in WT (Cre-negative) or *Zfp335<sup>fl/fl</sup> E8III-cre* (Zfp335cKO) mice. Total  
 469 numbers (C) and frequency (D) of TCR $\gamma\delta^+$  cells in WT or Zfp335cKO thymuses. Numbers (E)  
 470 and frequencies (F) of DN, DP, and SP thymocyte subsets in WT or Zfp335cKO thymuses.  
 471 Numbers (G) and frequencies (H) of early DN1-DN4 thymocyte subsets in WT or Zfp335cKO  
 472 thymuses. (I) Relative cells numbers in DN3-SP thymocyte subsets represented as percent of  
 473 WT mean. (J) Differential expression of select Zfp335-target genes by RNA-seq. (K) Overlap  
 474 between Zfp335 ChIP-seq (GSE58293) and differentially expressed genes in Zfp335cKO and

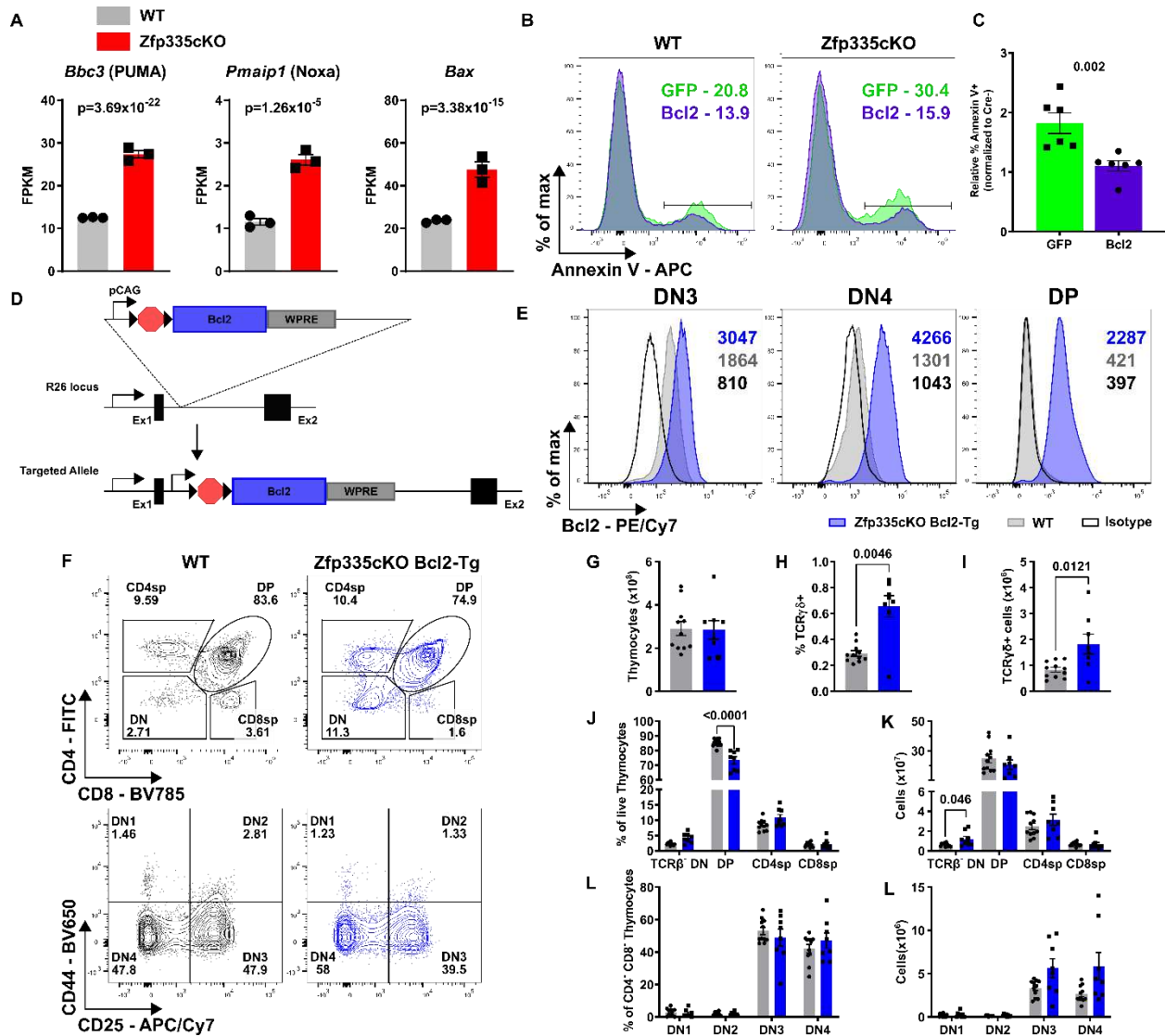
475 WT DP. (L) Gene Set Enrichment Analysis of differentially expressed genes (K). Positive  
476 enrichment scores indicate pathways positively enriched in Zfp335cKO cells. (A-K) Cre-negative  
477 WT (n=11) and Zfp335cKO (n=12) 4-5-week-old male and female mice from four independent  
478 experiments. *P*-values determined by Two-way ANOVA with *post hoc* Sidak test. (I-K) RNA-seq  
479 analysis of *Zfp335<sup>+/+</sup> E8<sub>III</sub>-cre* or Zfp335cKO DP thymocytes (n=3 each) of 6-week-old female  
480 mice from one experiment. Plots show mean  $\pm$  sem.



481

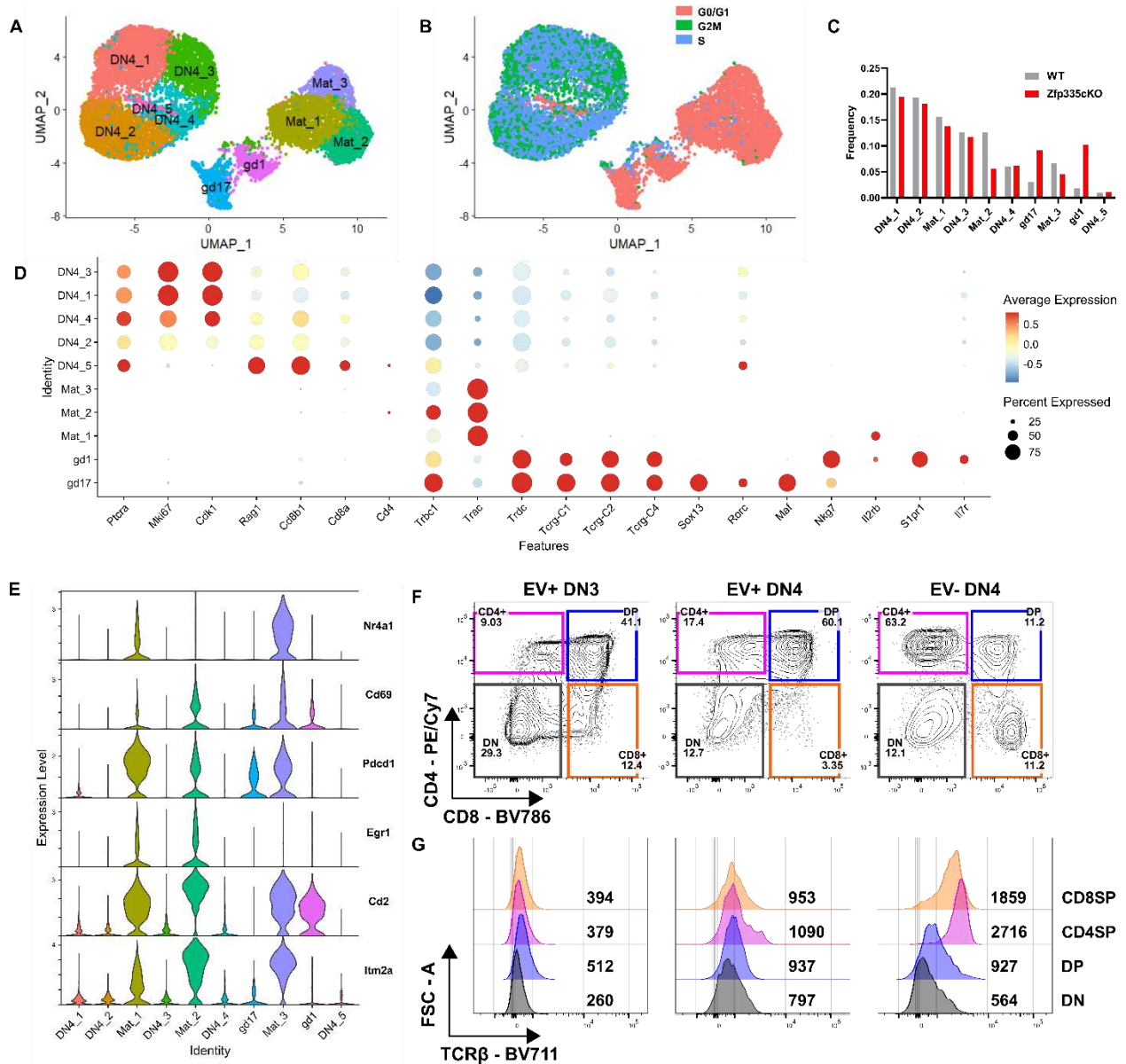
482 **Figure 2 - Zfp335cKO DN4 thymocytes undergo increased rates of apoptosis. (A-B)**  
 483 Assessment of developmental progression throughout OP9-DL1 culture. Proliferation

484 assessment (C-D) by Cell Trace Violet (CTV) dilution and apoptosis analysis (E-F) based on  
485 Annexin V binding at day3, 5 or 7 of culture. (G) Representative comparison of CTV dilution  
486 between Annexin V<sup>+</sup> and viable (DAPI<sup>-</sup> Annexin V<sup>-</sup>) cells on day 5 of culture. Representative  
487 CD4 vs CD8 expression among Annexin V<sup>+</sup> cells on day 5 of culture. n=6 WT or n=5  
488 Zfp335cKO from three independent experiments. *P*-values determined using Two-way  
489 Repeated Measures ANOVA with *post hoc* Sidak Test. Plots show mean  $\pm$  sem.



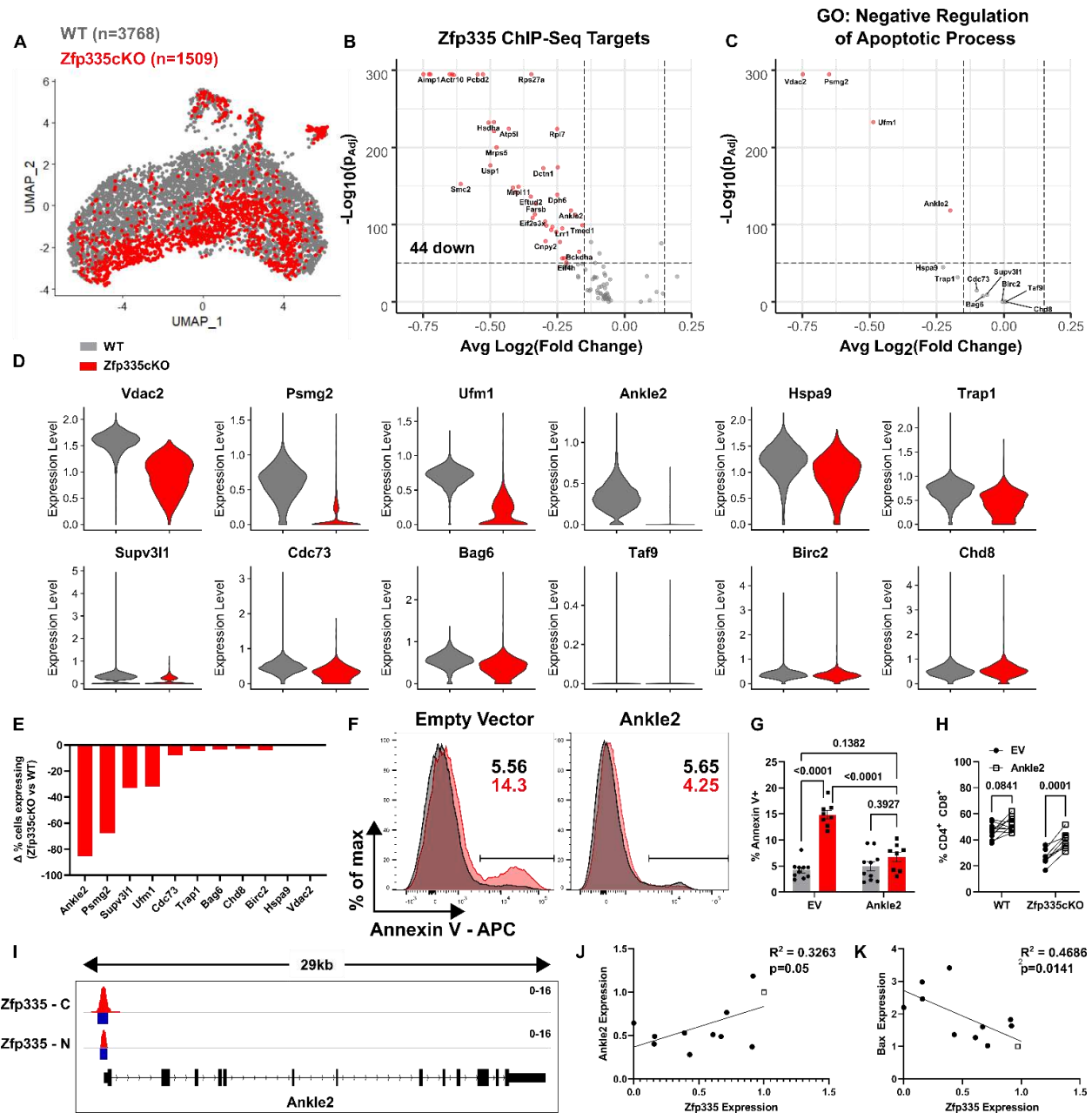
490

491 **Figure 3 – Bcl2 overexpression rescues Zfp335-deficient thymocytes from apoptosis.** (A)  
 492 Expression of pro-apoptotic Bcl2 family genes *Bbc3*, *Pmaip1*, or *Bax* from RNA-seq of control or  
 493 *Zfp335<sup>fl/fl</sup> E8III-cre* DP thymocytes. Representative gating (B) and quantification of apoptosis  
 494 among *Zfp335<sup>fl/fl</sup> E8III-cre* thymocytes transduced with Bcl2 or GFP RV after 5 days of OP9-DL1  
 495 culture (n=5). (E) Representative expression of isotype control (open black) or Bcl2 in WT (grey)  
 496 or *Zfp335<sup>fl/fl</sup> R26<sup>LSL-Bcl2</sup> E8III-cre* (blue) DN3, DN4 or DP thymocytes. (F) Gating for identification  
 497 of thymocyte subsets in WT WT (grey) or *Zfp335<sup>fl/fl</sup> R26<sup>LSL-Bcl2</sup> E8III-cre* (blue) mice. DN1-4 gating  
 498 pre-gated on TCR $\beta^+$ . (G) Total thymocyte numbers. Total numbers (H) and proportions (I) of  
 499 TCR $\delta^+$  cells. Frequencies (J) and total numbers (K) of DN, DP, CD4-SP and CD8-SP  
 500 thymocytes. Frequencies (L) and total numbers (M) of DN1-DN4 thymocytes. (F-M) n=11 WT or  
 501 n=8 *Zfp335<sup>fl/fl</sup> R26<sup>LSL-Bcl2</sup> E8III-cre*. Data compiled from one (A), two (B-C) or five (D-L)  
 502 independent experiments. P-values determined by Wald test (A), Mann-Whitney U-test (C) or  
 503 Two-way ANOVA with *post hoc* Sidak's test (H-M). Plots show mean  $\pm$  sem.



504

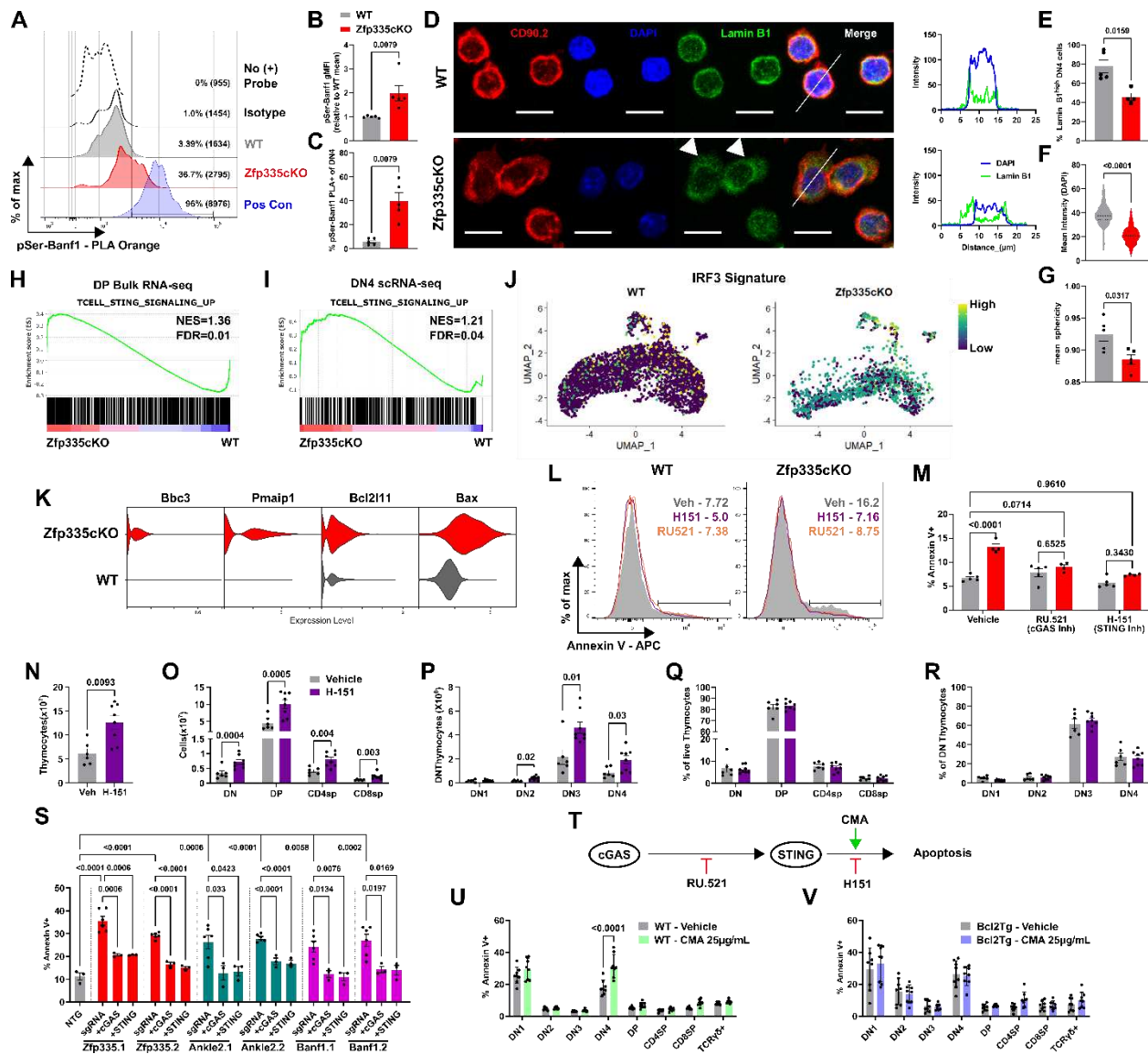
505 **Figure 4 – Defining the ‘true’ DN4 thymocyte population at the single cell level.** (A) UMAP  
 506 projection and identification of 10 clusters identified in full scRNA-seq dataset. (B) UMAP  
 507 colored by cell cycle phase. Blue or green identify actively cycling cells. (C) Frequency  
 508 distributions for WT (n=6357) and Zfp335cKO (n=5392) cells across the ten clusters. (D) Dot  
 509 plot of key cell type-defining genes. (E) Violin plots of positive selection signature genes in  
 510 thymocytes (Mingueneau et al. 2013). (F) Representative gating for CD4 vs. CD8 expression on  
 511 day 3 of OP9-DL1 cultures seeded with WT Thy1.1 retrovirus transduced (EV+) DN3 or DN4  
 512 cells or non-transduced (EV-) DN4 cells. (G) Representative TCRβ expression among DN, DP,  
 513 CD4SP or CD8SP cells from (F). Numbers indicate geometric MFI of TCRβ expression. (F-G)  
 514 Data representative of two independent experiments.



515

516 **Figure 5 – scRNA-seq identifies Ankle2 as a critical Zfp335-regulated gene controlling**  
 517 **survival of DN4 thymocytes.** (A) Violin plot of gene set score for Zfp335 target genes down-  
 518 regulated in mutant DP thymocytes (Fig 1L-M) and cutoff value used to identify true Zfp335  
 519 mutant cells (black box). (B) UMAP projections colored by genotype. Volcano plot of all  
 520 differentially expressed Zfp335 target genes (C) or those experimentally shown negatively  
 521 regulate apoptotic processes (D) between Zfp335 mutant and WT cells. (E) Violin plots of anti-  
 522 apoptotic Zfp335 target gene expression between Zfp335 mutant and WT DN4 cells. (F)  
 523 Differential proportions of Zfp335 mutant cells expressing anti-apoptotic genes from E compared  
 524 to WT cells. Representative gating (F) and quantification of apoptosis (G) or DP cell frequency  
 525 (H) for EV or Ankle2 retrovirus transduced WT (n=10) or Zfp335cKO (n=8) DN3 thymocytes  
 526 cultured on OP9-DL1 cells for 3 days. (I) Zfp335 ChIP-seq track of *Ankle2* locus in WT  
 527 thymocytes (Zfp335-C or Zfp335-N antibodies, GSE58293). Blue boxes indicate significant

528 binding peaks. Correlation between Ankle2 (J) or Bax (K) and Zfp335 expression in  
529 Scid.adh.2c2.SunTag CRISPRi cells expressing non-targeting (open squares) or Zfp335-  
530 targeting (closed circles) gRNAs. Data are compiled from one (A-E), two (J-K) or three (F-H)  
531 independent experiments. *P*-values determined by Wilcoxon Rank Sum test (B-C), two-way  
532 ANOVA with *post hoc* Tukey's test for multiple comparisons (G), repeated measures ANOVA  
533 with Sidak's test (H) or simple linear regression (J-K). Plots show mean  $\pm$  sem.



534

535 **Figure 6 – The Zfp335/Ankle2/Baf axis suppresses cGAS/STING-mediated apoptosis of**  
 536 **DN4 thymocytes.** (A) Representative histograms and gating of Baf phosphorylation as  
 537 measured by proximity ligation assay (PLA). Percent phosphoserine-Baf and geometric MFI in  
 538 parentheses are shown. Phosphoserine-Lamin B1 PLA was used as positive control.  
 539 Quantification of Baf phosphorylation based on geometric MFI (B) or percent positive cells (C).  
 540 (D) Representative immunofluorescence images of full cell thickness maximum intensity  
 541 projections (left) and profile plots (right) of nuclear envelope staining in *ex vivo* DN4 thymocytes.  
 542 Profile plots are based on white lines shown in merged images. Scale bars represent 10µm.  
 543 Quantification of frequency of cells with high nuclear-associated Lamin B1 (E), mean DAPI pixel  
 544 intensity (F) or mean nucleus sphericity (G) for *ex vivo* DN4 thymocytes. GSEA enrichment plots  
 545 for T cell-specific STING signaling gene signature in DP bulk (H) or DN4 scRNA-seq data sets  
 546 (I). (J) UMAP projection of IRF3 gene signature in WT or Zfp335 mutant DN4 thymocytes. (K)  
 547 Violin plots of pro-apoptotic Bcl2 gene expression in WT or Zfp335 mutant DN4 thymocytes.  
 548 Representative histograms (L) and quantification (M) of Annexin V-binding for WT or  
 549 Zfp335cKO DN4 thymocytes treated with cGAS (RU.521) or STING (H-151) inhibitors or vehicle

550 control and cultured on OP9-DL1 stromal cells for three days. Total thymocyte (N), DN, DP,  
551 CD4SP and CD8SP or DN1-DN4 cell numbers (O,P) or frequencies (Q,R) for Zfp335cKO mice  
552 treated with H-151 or vehicle *in vivo* for 7 days. (I-J) Thymocyte subset proportions for H-151 or  
553 vehicle treated Zfp335cKO mice. (S) Quantification of Annexin V binding among DN4 cells from  
554 R26<sup>LSL-Cas9</sup> Tcrd<sup>CreERT2</sup> thymocytes transduced with gRNA-expressing retroviruses and cultured  
555 for three days on OP9-DL1 cells with 4-hydroxytamoxifen. (T) Schematic diagram of inhibitors  
556 (RU.521 or H-151) or agonists (CMA) used to study cGAS/STING-dependent apoptosis of DN4  
557 thymocytes. Percent apoptosis induced by small molecule activation of STING among WT (U)  
558 or Zfp335cKO Bcl2Tg (V) thymocyte subsets. Values calculated by subtracting % Annexin V+ of  
559 vehicle-treated from % Annexin V+ of STING agonist-treated for each sample. *P*-values  
560 determined by Mann Whitney U-test (B-G,N) or two-way ANOVA with *post hoc* Tukey's test (M)  
561 or Sidak's test (O-P,U,V) or one-way ANOVA with *post hoc* Tukey's test (S). Data shown are  
562 compiled from one (H-K), two (L-M), three (A-G,U,V) or five (N-R) independent experiments.  
563 Plots show mean  $\pm$  sem or mean and interquartile range (F).

564

565

## 566 **Methods**

### 567 Mice

568 B6.Cg-Zfp335<sup>tm1Caw</sup> (Zfp335<sup>fl/fl</sup>, Stock No. 022413) and B6J.129(B6N)-  
569 Gt(ROSA)26Sor<sup>tm1(CAG-cas9\*,-EGFP)Fezh/J</sup> (R26<sup>LSL-Cas9</sup>, Stock No. 026175) mice were  
570 purchased from The Jackson Laboratory. C57BL/6J-Tg(Cd8a<sup>\*</sup>-cre)B6Asin (E8III-cre)  
571 mice were generously provided by Jung-Hyun Park (NIH). B6.129S-Tcrd<sup>tm1.1(cre/ERT2)Zhu</sup>  
572 (Tcrd<sup>CreERT2</sup>) have been maintained in our colony since original development. A modified  
573 Ai6 targeting vector to drive conditional overexpression of Bcl2 was generated by  
574 cloning in mouse *Bcl2* cDNA (Transomic Technologies) using FseI and SfiI restriction  
575 sites. R26<sup>LSL-Bcl2</sup> mice were generated by the Duke University Transgenic Facility using  
576 G4 mouse embryonic stem cells. Animals were maintained under specific pathogen-free  
577 conditions at the Cancer Center Isolation Facility of Duke University Medical Center. All  
578 experimental procedures were approved by the Institutional Animal Care and Use

579 Committee. All mice used in this study were 4-8 weeks old. For all experiments Cre-  
580 negative littermate controls were used unless otherwise stated.

### 581 Antibodies

582 All antibodies used in this study were purchased commercially and have previously  
583 been validated. Anti-TCR $\gamma\delta$  (GL3) was purchased from BD Biosciences. Anti- TCR $\gamma\delta$   
584 (GL3), rabbit anti-Lamin B (10H34L18), polyclonal rabbit anti-Banf1 (Cat. PA5-20329)  
585 and goat anti-rabbit IgG (H+L)-Alexa Fluor 647 were purchased from ThermoFisher  
586 Scientific. Anti-CD16/32 (2.4G2) was purchased from Tonbo Biosciences. Anti-CD90.1  
587 (OX7), anti-CD90.2 (30-H12), anti-CD4 (RM4-5), anti-CD8 (53-6.7), anti-CD44 (IM7),  
588 anti-CD25 (PC61), anti-CD62L (MEL-14), anti-TCR $\beta$  (H57-597), anti-CD27 (LG.3A10),  
589 anti-Bcl2 (BCL/10C4), anti-CD24 (M1/69), anti-B220 (RA3-6B2), anti-CD11b (M1/70),  
590 anti-CD11c (N418), anti-CD19 (6D5), anti-Ly6G/Ly6C (RB6-8C5), anti-NK1.1 (PK136),  
591 anti-TER119 (TER-119), anti-CD117/c-kit (2B8), anti-Phosphoserine (M380B), mouse  
592 IgG1 isotype control (MG1-45), mouse IgG1 isotype control (MOPC-21) and Annexin V  
593 were purchased from Biolegend.

### 594 Flow cytometry and cell sorting

595 Thymus or spleen tissues were harvested from 4-8 week old mice. Tissues were then  
596 dissociated in FACS Buffer (PBS supplemented with 2.5% FBS and 2mM EDTA) using  
597 a Dounce Homogenizer and filtered through 70 $\mu$ m nylon mesh (Genesee Scientific) to  
598 yield single-cell suspensions. For spleen samples, red blood cells were lysed using 1x  
599 RBC lysis buffer then resuspended in FACS buffer. 0.5-1x10<sup>7</sup> cells were stained with  
600 fluorescently labelled antibodies for 30 minutes at 4°C then washed with excess FACS

601 buffer. Prior to analysis propidium iodide (Sigma-Aldrich, Cat. P4170) or DAPI (Sigma-  
602 Aldrich, Cat. D9542) were added to a final concentration of 0.5 $\mu$ g/mL or 100ng/mL,  
603 respectively for live/ dead discrimination. Cells were analyzed on a Fortessa X20 (BD  
604 Biosciences) or FACSCantoII (BD Biosciences) cytometer. For isolation of thymocyte  
605 subsets or virally transduced cells, sorting was performed using a FACSDiva (BD  
606 Biosciences) or Astrios (Beckman-Coulter) cell sorter. For sorting of thymocyte subsets  
607 *ex vivo*, staining included a lineage dump stain consisting of B220, CD11b, CD11c,  
608 CD19, GR-1, NK1.1, TCR $\beta$ , TCR $\gamma\delta$  and TER119 antibodies. All analyses were  
609 performed using FlowJo v10 software (TreeStar). Detailed gating schemes are shown in  
610 Supp. Fig 7.

#### 611 Bulk RNA-seq

612 DP thymocytes (Lin<sup>-</sup> CD4<sup>+</sup> CD8<sup>+</sup>) were FACS sorted from total thymus of 7-week-old  
613 female Zfp335<sup>fl/fl</sup> E8<sup>III-cre</sup> or Zfp335<sup>+/+</sup> E8<sup>III-cre</sup> mice. Purified DP cells were lysed with  
614 Trizol and RNA isolated using the DirectZol Micro RNA prep kit (Zymo) according to  
615 manufacturer's recommended protocol. gDNA was eliminated by on-column DNase  
616 digestion. Libraries were prepared using standard preparation protocols by BGI  
617 Genomics. 150bp paired-end sequencing was performed on the BGISEQ-500  
618 sequencing platform.

619 Paired-end reads were mapped to the mouse mm10 reference genome using the  
620 HiSat2 software and count matrices generated using the featureCounts function of the  
621 Subreads software package. Differential expression analysis was performed using  
622 edgeR and DeSeq2 implemented through iDep.91  
623 (<http://bioinformatics.sdstate.edu/idep90/>). Gene-Set Enrichment Analysis (GSEA) was

624 utilized to identify enriched pathways based on differential expression analysis using  
625 pre-ranked gene lists.

## 626 Cell Culture

627 OP9-DL1 cells, kindly provided by Maria Ciofani (Duke University) were cultured in  
628 MEM $\alpha$  (Gibco) supplemented with 10% FBS (Atlanta Biologicals) and 1x penicillin/  
629 streptomycin (Gibco). HEK293T cells were cultured in DMEM supplemented with 10%  
630 FBS, 1x penicillin/ streptomycin, 1x non-essential amino acids and 1x GlutaMAX. For  
631 OP9-DL1 culture of thymocytes, cultures were additionally supplemented with 5ng/mL  
632 recombinant mouse IL-7 (Biolegend). Scid.adh.2c2 cells were cultured in IMDM  
633 supplemented with 10% FBS (Hyclone), 1x penicillin/ streptomycin, 1x NEAA, 1x  
634 sodium pyruvate, 1x GlutaMAX, and 55 $\mu$ M  $\beta$ -mercaptoethanol. In some OP9-DL1  
635 cultures 5 $\mu$ g/mL RU.521 (Invivogen), 0.5 $\mu$ g/mL H-151 (Cayman Chemicals) or 25 $\mu$ g/mL  
636 Cridanimod (Cayman Chemicals) were added. All cultures were maintained at 37°C with  
637 5% CO<sub>2</sub>.

## 638 DN thymocyte enrichment

639 Total thymocytes were harvested from 4–8-week-old mice. Tissues were dissociated  
640 and strained through 30 $\mu$ m nylon mesh (Genesee Scientific). For purification of DN3/4  
641 thymocytes cells were stained with biotinylated antibodies against B220, CD3, CD4,  
642 CD8, CD11b, CD11c, CD19, CD44, c-Kit, GR-1, IgM, NK1.1, TCR $\beta$ , and TCR $\gamma\delta$ . For  
643 enrichment of total DN cells CD44 and c-Kit antibodies were excluded. Following  
644 antibody staining, cells were incubated with 50 $\mu$ L or 100 $\mu$ L of streptavidin magnetic  
645 particles (Spherotech, cat. SVM-40-100) / 10<sup>7</sup> cells at 2 x 10<sup>7</sup> cells/mL in FACS buffer

646 for total DN enrichment or DN3/4 purification, respectively. Particle-bound cells were  
647 separated three times on a magnetic rack.

#### 648 Retrovirus packaging and transduction

649 Retrovirus were generated by transfecting HEK293T cells with 1 $\mu$ g/mL each of MSCV  
650 transfer and pCL-Eco vectors using Lipofectamine 2000 (Invitrogen) or JetOptimus  
651 (Genesee Scientific) according to manufacturer's recommended protocols. Media was  
652 changed 24 hours post-transfection and viral supernatants harvested 24 hours later.  
653 DN3/4-enriched thymocytes were transduced with fresh viral supernatant via spinfection  
654 for 2 hours at 2300 rpm at 30°C with 6.7 $\mu$ g/mL polybrene (Millipore). Following  
655 spinfection cells were transferred to culture on OP9-DL1 stromal cells for overnight  
656 culture. 18-24 hours post-infection virally transduced (DsRed<sup>+</sup> or Thy1.1<sup>+</sup>) DN3  
657 (CD25<sup>+</sup>) or DN4 (CD25<sup>-</sup>) were isolated by FACS sorting for an additional 3-5 days of  
658 culture in the OP9-DL1 culture system. For dual-targeting CRISPR experiments, equal  
659 volumes of sgRNA-Thy1.1 and -DsRed viral supernatants were mixed for transduction.

#### 660 scRNA-seq library preparation

661 For single cell RNA-sequencing, DN4 thymocytes (Live Lin<sup>-</sup> CD4<sup>-</sup> CD8<sup>-</sup> CD25<sup>-</sup> CD44<sup>-</sup>)  
662 were sorted from one male and one female mouse pooled for each genotype using an  
663 Astrios Sorter. Sorted cells were encapsulated into droplets and libraries were prepared  
664 using a Chromium Single Cell 3' Kit using the v3.1 chemistry. 7,000 cells per genotype  
665 were targeted. scRNA-seq libraries were pooled and sequenced on a NovaSeq S Prime  
666 Flow Cell yielding an average depth of 71,584 or 67,816 reads per cells for Zfp335cKO  
667 or WT samples, respectively.

668 scRNA-seq analysis

669 scRNA-seq data were processed using the Cell Ranger pipeline (10x Genomics).  
670 FASTQ files were generated from raw base call logs (bcl2fastq, v2.20), aligned to the  
671 mouse mm10 (release 93) reference genome (cellranger, v3.1.0; STAR v2.5.3a) to  
672 generate raw gene count matrices.

673 All downstream analyses were performed using the R software package Seurat (v4.0.0).  
674 Data was filtered to exclude cells with < 1,000 genes detected or < 1,000 UMIs.  
675 Doublets were excluded by filtering cells with > 60,000 UMIs. Low-quality cells were  
676 further filtered by removal of cells with > 7.5% mitochondrial gene expression. Gene  
677 expression matrices were then merged, data normalized, scaled and cell cycle scored  
678 using standard methods with Seurat. Dropouts were imputed using the R package  
679 ALRA. Cell cycle phase was regressed, and principal component analysis (PCA) was  
680 performed on the 6,000 most variable genes. 35 principal components were selected for  
681 downstream analysis based on JackStraw analysis. Dimensionality reduction was  
682 performed by Uniform Manifold Approximation and Projection (UMAP) and clustering  
683 defined using a resolution of 0.5. Gene expression was visualized by VlnPlot, DotPlot  
684 and FeaturePlot functions in Seurat. Gene signature scores were calculated using  
685 SingleCellSignatureExplorer and previously described methods<sup>69</sup>. Differential  
686 expression analysis was performed using the FindMarkers function in Seurat with  
687 Wilcoxon Rank Sum Test.

688 Cloning cDNA overexpression vectors

689 Bcl2 overexpression vector was generated by cloning Bcl2 cDNA (Transomic  
690 Technologies, Cat. TCM1304) into the pMSCV-loxp-dsRed-loxP-eGFP-puro-WPRE  
691 vector (Addgene #32702) using the EcoRI and NsiI restriction sites. Ankle2 cDNA  
692 (Transomic Technologies, Cat. TCM1004) was cloned into the MSCV-IRES-Thy1.1  
693 vector using NEBuilder Hifi Assembly (New England Biolabs). All vectors were  
694 propagated in Stbl3 cells (ThermoFisher Scientific).

#### 695 Generation of *Scid.adh.2c2-dCas9<sup>10x-GCN4</sup>* CRISPRi cells

696 dCas9<sup>10x-GCN4</sup> (pHRdSV40-dCas9-10xGCN4\_v4-P2A-BFP, Addgene #60904) was  
697 lentivirally transduced into *Scid.adh.2c2* cells, following which BFP+ cells were isolated  
698 by flow cytometry. Single cells were then cloned into 96 well plates and screened for  
699 knockdown efficiency using CD25 gRNA retroviral vectors. Clones exhibiting more than  
700 90% CD25 downmodulation were expanded for use in our studies.

#### 701 Generation of gRNA retroviral vectors

702 All gRNAs were designed using the CRISPick<sup>70</sup> gRNA design tool. All gRNAs were  
703 cloned into expression vectors by annealing followed by ligation into a BbsI cleavage  
704 site. The basic gRNA expression vector used was the MSCV-mU6-sgRNA-hPGK-  
705 Thy1.1 (kindly provided by Maria Ciofani). Knock-out gRNAs were first cloned into this  
706 Thy1.1 backbone. To generate DsRed expressing vectors for dual targeting, Thy1.1  
707 was removed by digestion with BamHI and EcoRI and replaced with DsRed Express II  
708 by NEBuilder Hifi Assembly. The CRISRPi retroviral vector was generated by first  
709 cloning the pSV40-scFv-GCN4-sfGFP-VP64-GB1-NLS (Addgene #60904) fusion

710 construct into the MSCV-mU6-sgRNA-hPGK backbone followed by replacement of  
711 VP64 with KRAB using NEBuilder.

#### 712 qPCR analysis of gene expression

713 Following viral transduction, Scid.adh.2c2.dCas9<sup>10x-GCN4</sup> cells were assessed for  
714 transduction efficiency by flow cytometry. For samples exceeding 90% GFP+ 10<sup>6</sup> cells  
715 were lysed in Trizol and RNA isolated using the Direct-Zol MicroPrep kit. 500ng of RNA  
716 was reverse transcribed using SuperScript III Reverse Transcriptase (Invitrogen) with  
717 random hexamers according to the manufacturer's recommended protocol. 5ng of  
718 cDNA per 25µL reaction was then used for gene expression analysis with PowerTrack  
719 Sybr Green Master Mix (Applied Biosciences) according to the manufacturer's  
720 recommended protocol using fast cycling conditions with an Eppendorf MasterCycler  
721 qPCR machine. Relative expression was determined using the ddCt method with  
722 Gapdh being used for normalization.

#### 723 Proximity Ligation Assay for Baf phosphorylation

724 Proximity ligation assays were performed using the Duolink<sup>®</sup> flowPLA Detection  
725 Kit – Orange (Millipore Sigma, Cat. DUO94003) according to manufacturers  
726 recommended protocol with minor changes. Briefly, total thymocytes were prepared as  
727 described in flow cytometry and cell sorting methods section. 10<sup>7</sup> thymocytes were  
728 stained with surface antibodies to distinguish all major thymocyte subsets. Next, cells  
729 were fixed with 4% paraformaldehyde for 10 minutes, washed and permeabilized for 30  
730 minutes at room temperature. After permeabilization, cells were blocked for 1 hour at  
731 37°C with 300µl of Duolink<sup>®</sup> blocking solution then stained overnight at 4°C with purified

732 mouse anti-Phosphoserine (Biolegend) or purified mouse IgG1 isotype control (clone  
733 MG1-45, Biolegend) and purified rabbit anti-Banf1 (ThermoFisher Scientific) or rabbit  
734 anti-Lamin B1 (ThermoFisher Scientific) diluted in Duolink<sup>®</sup> antibody diluent. After each  
735 step cells were washed twice with 1mL of Duolink<sup>®</sup> In Situ wash buffer. Next, cells were  
736 incubated for 1 hour at 37°C with Duolink<sup>®</sup> In Situ PLA<sup>®</sup> Probe Anti-Rabbit PLUS (Sigma  
737 Millipore, Cat. DUO92002) and Duolink<sup>®</sup> In Situ PLA<sup>®</sup> Probe Anti-Mouse MINUS (Sigma  
738 Millipore, Cat. DUO92004) diluted in Duolink<sup>®</sup> antibody diluent. Additional controls in  
739 which individual probes were omitted were also prepared. Following probe incubation,  
740 cells were washed then incubated for 30 minutes at 37°C with 1x Duolink<sup>®</sup> ligation  
741 reaction mixture, washed again and incubated for 90 minutes with 1x Duolink<sup>®</sup>  
742 amplification reaction mixture. Following amplification, cells were incubated with 1x  
743 Duolink<sup>®</sup> Detection Solution – Orange for 15 minutes at 37°C. Cells were finally washed,  
744 resuspended in PBS and assayed using a FortessaX20 cytometer (BD Biosciences).

#### 745 Determination of nuclear envelope structure

746  $5 \times 10^4$  HeLa cells per well were reverse transfected with 15pmol siRNA using  
747 Lipofectamine RNAiMax (ThermoFisher Scientific) in an 8 well chamber slide according  
748 to recommended protocols. ANKLE2 and universal non-targeting control siRNAs were  
749 purchased from IDT (Design ID: hs.Ri.ANKLE2.13). BANF-targeting siRNAs were  
750 purchased from ThermoFisher Scientific (IDs: s16807, s16808, 26065). 48 hours post-  
751 transfection cells were fixed with 4% paraformaldehyde for 10 minutes at room  
752 temperature and permeabilized with permeabilization buffer for 1h at RT temperature.  
753 Primary antibody Lamin B (Invitrogen, Cat. 702972) were added for overnight incubation  
754 at 4°C and washed with 1X PBS for three times. After that, secondary antibody Alexa

755 Fluor 647-conjugated goat anti-rabbit antibody (Invitrogen, Cat. A32733) were added for  
756 12h at 4C in the dark. After washing with 1X PBS for three times, slides were mounted  
757 with DAPI-containing mounting media (VECTORLAB, Cat. H-1200). Images were  
758 collected using Zeiss 780 upright confocal. To analyze nuclear structure DAPI channel  
759 images were converted to binary with ImageJ. Following binarization, the Watershed  
760 function was used to separate touching cells. Circularity was then determined with a  
761 minimum threshold of 500 px<sup>2</sup>.

762 For analysis of *ex vivo* DN4 thymocyte nuclear envelope DN4 cells were  
763 isolated by magnetic bead-based purification. Following purification, cells were fixed  
764 with 4% paraformaldehyde for 10 minutes at room temperature. Cells were then  
765 stained overnight with purified rabbit anti-Lamin B1 antibody, followed by  
766 incubation with goat anti-rabbit AlexaFluor 488 secondary antibody (ThermoFisher  
767 Scientific) for 1 hour. Cells were spun onto slides using the CytoSpin4 centrifuge  
768 (ThermoFisher Scientific) and mounted with ProLong™ Gold Antifade Mountant with  
769 DAPI (ThermoFisher Scientific). Microscopy images were acquired on the Zeiss 710  
770 Inverted Laser Scanning Confocal Microscope (Duke University Light Microscopy Core  
771 Facility). For quantification, at least 20 cells per animal were imaged as z-stacks using  
772 the 63x oil immersion objective. Image quantification was conducted with the Imaris  
773 for Neuroscientists Cell Imaging Software v. 9.3.0 (Bitplane) using the Surfaces tool  
774 on the acquired DAPI signal to identify nuclei. Identified nuclei were then  
775 differentiated by mean fluorescent intensity of Lamin B1, and quantified. The

776 percentage of nuclei identified as Lamin B1<sup>high</sup> and mean sphericity of all nuclei for  
777 each animal was used as a single n for statistical analysis. Additionally, mean DAPI  
778 intensity was quantified for individual nuclei, with each nucleus represented as a  
779 single data point.

#### 780 *In vivo* H-151 treatment of mice

781 Mice were administered 750 pmol (210µg) of H-151 (Cayman Chemicals) or vehicle via  
782 intraperitoneal injection daily for 7 days beginning at 7 weeks of age. The vehicle for  
783 injections was sterile PBS + 10% Tween-80 (VWR).

#### 784 Statistical analysis

785 Statistical tests were performed using GraphPad v9.0.0 (Prism). For graphs with  
786 multiple comparisons being made, two-way ANOVA was performed with post-hoc  
787 Sidak's test or Tukey's test for multiple comparisons. For comparisons of cell numbers,  
788 data was log transformed prior to statistical tests. For all Two-way ANOVA tests  
789 normality tests were performed to ensure normalcy assumptions were met. For graphs  
790 of single comparisons, a two-tailed Mann-Whitney test was used. All significant p-values  
791 are shown in each graph. No statistical methods were used to predetermine sample  
792 size.

#### 793 **Data and code availability**

794 Data generated in this study can be accessed upon publication through NCBI Gene  
795 Expression Omnibus (<https://www.ncbi.nlm.nih.gov/geo/>) under accession GSE189244.  
796 All code from this study is available upon request.

797 **References**

798 1. Krueger, A., Zietara, N. & Lyszkiewicz, M. T Cell Development by the Numbers. *Trends Immunol*  
799 **38**, 128-139 (2017).

800

801 2. Li, L., Leid, M. & Rothenberg, E.V. An early T cell lineage commitment checkpoint dependent on  
802 the transcription factor Bcl11b. *Science* **329**, 89-93 (2010).

803

804 3. Tourigny, M.R., Mazel, S., Burtrum, D.B. & Petrie, H.T. T cell receptor (TCR)-beta gene  
805 recombination: dissociation from cell cycle regulation and developmental progression during T  
806 cell ontogeny. *J Exp Med* **185**, 1549-1556 (1997).

807

808 4. Wojciechowski, J., Lai, A., Kondo, M. & Zhuang, Y. E2A and HEB are required to block thymocyte  
809 proliferation prior to pre-TCR expression. *J Immunol* **178**, 5717-5726 (2007).

810

811 5. Boudil, A. *et al.* IL-7 coordinates proliferation, differentiation and Tcr $\alpha$  recombination during  
812 thymocyte beta-selection. *Nat Immunol* **16**, 397-405 (2015).

813

814 6. Kelly, A.P. *et al.* Notch-induced T cell development requires phosphoinositide-dependent kinase  
815 1. *EMBO J* **26**, 3441-3450 (2007).

816

817 7. Guidos, C.J. Synergy between the pre-T cell receptor and Notch: cementing the alphabeta  
818 lineage choice. *J Exp Med* **203**, 2233-2237 (2006).

819

820 8. Yamasaki, S. *et al.* Mechanistic basis of pre-T cell receptor-mediated autonomous signaling  
821 critical for thymocyte development. *Nat Immunol* **7**, 67-75 (2006).

822

823 9. Fehling, H.J., Krotkova, A., Saint-Ruf, C. & von Boehmer, H. Crucial role of the pre-T-cell receptor  
824 alpha gene in development of alpha beta but not gamma delta T cells. *Nature* **375**, 795-798  
825 (1995).

826

827 10. Zhao, B. *et al.* Notch and the pre-TCR coordinate thymocyte proliferation by induction of the SCF  
828 subunits Fbx1 and Fbx12. *Nat Immunol* **20**, 1381-1392 (2019).

829

830 11. Chen, L., Foreman, D.P., Sant'Angelo, D.B. & Krangel, M.S. Yin Yang 1 Promotes Thymocyte  
831 Survival by Downregulating p53. *J Immunol* **196**, 2572-2582 (2016).

832

833 12. Bouillet, P. *et al.* BH3-only Bcl-2 family member Bim is required for apoptosis of autoreactive  
834 thymocytes. *Nature* **415**, 922-926 (2002).

835

- 836 13. Hutcheson, J. & Perlman, H. Loss of Bim results in abnormal accumulation of mature CD4-CD8-  
837 CD44-CD25- thymocytes. *Immunobiology* **212**, 629-636 (2007).
- 838  
839 14. Villunger, A. *et al.* p53- and drug-induced apoptotic responses mediated by BH3-only proteins  
840 puma and noxa. *Science* **302**, 1036-1038 (2003).
- 841  
842 15. Ren, D. *et al.* BID, BIM, and PUMA are essential for activation of the BAX- and BAK-dependent  
843 cell death program. *Science* **330**, 1390-1393 (2010).
- 844  
845 16. Hutcheson, J. *et al.* Combined loss of proapoptotic genes Bak or Bax with Bim synergizes to  
846 cause defects in hematopoiesis and in thymocyte apoptosis. *J Exp Med* **201**, 1949-1960 (2005).
- 847  
848 17. Rothenberg, E.V. & Taghon, T. Molecular genetics of T cell development. *Annu Rev Immunol* **23**,  
849 601-649 (2005).
- 850  
851 18. Sawada, S. & Littman, D.R. A heterodimer of HEB and an E12-related protein interacts with the  
852 CD4 enhancer and regulates its activity in T-cell lines. *Mol Cell Biol* **13**, 5620-5628 (1993).
- 853  
854 19. Belle, I. & Zhuang, Y. E proteins in lymphocyte development and lymphoid diseases. *Curr Top*  
855 *Dev Biol* **110**, 153-187 (2014).
- 856  
857 20. Hsu, L.Y. *et al.* A conserved transcriptional enhancer regulates RAG gene expression in  
858 developing B cells. *Immunity* **19**, 105-117 (2003).
- 859  
860 21. Herblot, S., Steff, A.M., Hugo, P., Aplan, P.D. & Hoang, T. SCL and LMO1 alter thymocyte  
861 differentiation: inhibition of E2A-HEB function and pre-T alpha chain expression. *Nat Immunol* **1**,  
862 138-144 (2000).
- 863  
864 22. Jia, J., Dai, M. & Zhuang, Y. E proteins are required to activate germline transcription of the TCR  
865 Vbeta8.2 gene. *Eur J Immunol* **38**, 2806-2820 (2008).
- 866  
867 23. Ghosh, J.K., Romanow, W.J. & Murre, C. Induction of a diverse T cell receptor gamma/delta  
868 repertoire by the helix-loop-helix proteins E2A and HEB in nonlymphoid cells. *J Exp Med* **193**,  
869 769-776 (2001).
- 870  
871 24. Jones, M.E. & Zhuang, Y. Stage-specific functions of E-proteins at the beta-selection and T-cell  
872 receptor checkpoints during thymocyte development. *Immunol Res* **49**, 202-215 (2011).
- 873  
874 25. Engel, I., Johns, C., Bain, G., Rivera, R.R. & Murre, C. Early thymocyte development is regulated  
875 by modulation of E2A protein activity. *J Exp Med* **194**, 733-745 (2001).

- 876  
877 26. Xu, W. *et al.* E2A transcription factors limit expression of Gata3 to facilitate T lymphocyte  
878 lineage commitment. *Blood* **121**, 1534-1542 (2013).
- 879  
880 27. Jones, M.E. & Zhuang, Y. Acquisition of a functional T cell receptor during T lymphocyte  
881 development is enforced by HEB and E2A transcription factors. *Immunity* **27**, 860-870 (2007).
- 882  
883 28. Kato, K., Omura, H., Ishitani, R. & Nureki, O. Cyclic GMP-AMP as an Endogenous Second  
884 Messenger in Innate Immune Signaling by Cytosolic DNA. *Annu Rev Biochem* **86**, 541-566 (2017).
- 885  
886 29. Sun, L., Wu, J., Du, F., Chen, X. & Chen, Z.J. Cyclic GMP-AMP synthase is a cytosolic DNA sensor  
887 that activates the type I interferon pathway. *Science* **339**, 786-791 (2013).
- 888  
889 30. Cerboni, S. *et al.* Intrinsic antiproliferative activity of the innate sensor STING in T lymphocytes. *J*  
890 *Exp Med* **214**, 1769-1785 (2017).
- 891  
892 31. Gulen, M.F. *et al.* Signalling strength determines proapoptotic functions of STING. *Nat Commun*  
893 **8**, 427 (2017).
- 894  
895 32. Li, W. *et al.* cGAS-STING-mediated DNA sensing maintains CD8(+) T cell stemness and promotes  
896 antitumor T cell therapy. *Sci Transl Med* **12** (2020).
- 897  
898 33. Wu, J., Dobbs, N., Yang, K. & Yan, N. Interferon-Independent Activities of Mammalian STING  
899 Mediate Antiviral Response and Tumor Immune Evasion. *Immunity* **53**, 115-126 e115 (2020).
- 900  
901 34. Yang, Y.J. *et al.* Microcephaly gene links trithorax and REST/NRSF to control neural stem cell  
902 proliferation and differentiation. *Cell* **151**, 1097-1112 (2012).
- 903  
904 35. Park, J.H. *et al.* Signaling by intrathymic cytokines, not T cell antigen receptors, specifies CD8  
905 lineage choice and promotes the differentiation of cytotoxic-lineage T cells. *Nat Immunol* **11**,  
906 257-264 (2010).
- 907  
908 36. Guey, B. *et al.* BAF restricts cGAS on nuclear DNA to prevent innate immune activation. *Science*  
909 **369**, 823-828 (2020).
- 910  
911 37. Engel, I. & Murre, C. The function of E- and Id proteins in lymphocyte development. *Nat Rev*  
912 *Immunol* **1**, 193-199 (2001).
- 913  
914 38. Engel, I. & Murre, C. E2A proteins enforce a proliferation checkpoint in developing thymocytes.  
915 *EMBO J* **23**, 202-211 (2004).

- 916  
917 39. Jones-Mason, M.E. *et al.* E protein transcription factors are required for the development of  
918 CD4(+) lineage T cells. *Immunity* **36**, 348-361 (2012).
- 919  
920 40. Roy, S. *et al.* Id Proteins Suppress E2A-Driven Invariant Natural Killer T Cell Development prior to  
921 TCR Selection. *Front Immunol* **9**, 42 (2018).
- 922  
923 41. Dashtsoodol, N. *et al.* Alternative pathway for the development of Valpha14(+) NKT cells directly  
924 from CD4(-)CD8(-) thymocytes that bypasses the CD4(+)CD8(+) stage. *Nat Immunol* **18**, 274-282  
925 (2017).
- 926  
927 42. Han, B.Y. *et al.* Zinc finger protein Zfp335 is required for the formation of the naive T cell  
928 compartment. *Elife* **3** (2014).
- 929  
930 43. Haks, M.C., Krimpenfort, P., van den Brakel, J.H. & Kruisbeek, A.M. Pre-TCR signaling and  
931 inactivation of p53 induces crucial cell survival pathways in pre-T cells. *Immunity* **11**, 91-101  
932 (1999).
- 933  
934 44. Taghon, T., Yui, M.A., Pant, R., Diamond, R.A. & Rothenberg, E.V. Developmental and molecular  
935 characterization of emerging beta- and gammadelta-selected pre-T cells in the adult mouse  
936 thymus. *Immunity* **24**, 53-64 (2006).
- 937  
938 45. Holmes, R. & Zuniga-Pflucker, J.C. The OP9-DL1 system: generation of T-lymphocytes from  
939 embryonic or hematopoietic stem cells in vitro. *Cold Spring Harb Protoc* **2009**, pdb prot5156  
940 (2009).
- 941  
942 46. Mingueneau, M. *et al.* The transcriptional landscape of alphabeta T cell differentiation. *Nat*  
943 *Immunol* **14**, 619-632 (2013).
- 944  
945 47. Miller, D.G., Adam, M.A. & Miller, A.D. Gene transfer by retrovirus vectors occurs only in cells  
946 that are actively replicating at the time of infection. *Mol Cell Biol* **10**, 4239-4242 (1990).
- 947  
948 48. Trang, N.V. *et al.* Determination of cut-off cycle threshold values in routine RT-PCR assays to  
949 assist differential diagnosis of norovirus in children hospitalized for acute gastroenteritis.  
950 *Epidemiol Infect* **143**, 3292-3299 (2015).
- 951  
952 49. Asencio, C. *et al.* Coordination of kinase and phosphatase activities by Lem4 enables nuclear  
953 envelope reassembly during mitosis. *Cell* **150**, 122-135 (2012).
- 954

- 955 50. Carleton, M. *et al.* Signals transduced by CD3epsilon, but not by surface pre-TCR complexes, are  
956 able to induce maturation of an early thymic lymphoma in vitro. *J Immunol* **163**, 2576-2585  
957 (1999).
- 958
- 959 51. Tanenbaum, M.E., Gilbert, L.A., Qi, L.S., Weissman, J.S. & Vale, R.D. A protein-tagging system for  
960 signal amplification in gene expression and fluorescence imaging. *Cell* **159**, 635-646 (2014).
- 961
- 962 52. Ma, H. *et al.* Barrier-to-Autointegration Factor 1 Protects against a Basal cGAS-STING Response.  
963 *mBio* **11** (2020).
- 964
- 965 53. Larkin, B. *et al.* Cutting Edge: Activation of STING in T Cells Induces Type I IFN Responses and Cell  
966 Death. *J Immunol* **199**, 397-402 (2017).
- 967
- 968 54. Zierhut, C. & Funabiki, H. Regulation and Consequences of cGAS Activation by Self-DNA. *Trends*  
969 *Cell Biol* **30**, 594-605 (2020).
- 970
- 971 55. McArthur, K. *et al.* BAK/BAX macropores facilitate mitochondrial herniation and mtDNA efflux  
972 during apoptosis. *Science* **359** (2018).
- 973
- 974 56. Vincent, J. *et al.* Small molecule inhibition of cGAS reduces interferon expression in primary  
975 macrophages from autoimmune mice. *Nat Commun* **8**, 750 (2017).
- 976
- 977 57. Haag, S.M. *et al.* Targeting STING with covalent small-molecule inhibitors. *Nature* **559**, 269-273  
978 (2018).
- 979
- 980 58. Zhang, B. *et al.* Differential Requirements of TCR Signaling in Homeostatic Maintenance and  
981 Function of Dendritic Epidermal T Cells. *J Immunol* **195**, 4282-4291 (2015).
- 982
- 983 59. Lucas, B. & Germain, R.N. Unexpectedly complex regulation of CD4/CD8 coreceptor expression  
984 supports a revised model for CD4+CD8+ thymocyte differentiation. *Immunity* **5**, 461-477 (1996).
- 985
- 986 60. Agata, Y. *et al.* Regulation of T cell receptor beta gene rearrangements and allelic exclusion by  
987 the helix-loop-helix protein, E47. *Immunity* **27**, 871-884 (2007).
- 988
- 989 61. Petersson, K., Ivars, F. & Sigvardsson, M. The pT alpha promoter and enhancer are direct targets  
990 for transactivation by E box-binding proteins. *Eur J Immunol* **32**, 911-920 (2002).
- 991
- 992 62. Wang, D. *et al.* The basic helix-loop-helix transcription factor HEBAIt is expressed in pro-T cells  
993 and enhances the generation of T cell precursors. *J Immunol* **177**, 109-119 (2006).
- 994

995 63. Link, N. *et al.* Mutations in ANKLE2, a ZIKA Virus Target, Disrupt an Asymmetric Cell Division  
996 Pathway in Drosophila Neuroblasts to Cause Microcephaly. *Dev Cell* **51**, 713-729 e716 (2019).

997

998 64. Yamamoto, S. *et al.* A drosophila genetic resource of mutants to study mechanisms underlying  
999 human genetic diseases. *Cell* **159**, 200-214 (2014).

1000

1001 65. Matsui, T.K. & Mori, E. Microglia support neural stem cell maintenance and growth. *Biochem*  
1002 *Biophys Res Commun* **503**, 1880-1884 (2018).

1003

1004 66. Shigemoto-Mogami, Y., Hoshikawa, K., Goldman, J.E., Sekino, Y. & Sato, K. Microglia enhance  
1005 neurogenesis and oligodendrogenesis in the early postnatal subventricular zone. *J Neurosci* **34**,  
1006 2231-2243 (2014).

1007

1008 67. Ribeiro Xavier, A.L., Kress, B.T., Goldman, S.A., Lacerda de Menezes, J.R. & Nedergaard, M. A  
1009 Distinct Population of Microglia Supports Adult Neurogenesis in the Subventricular Zone. *J*  
1010 *Neurosci* **35**, 11848-11861 (2015).

1011

1012 68. Reinert, L.S. *et al.* Brain immune cells undergo cGAS/STING-dependent apoptosis during herpes  
1013 simplex virus type 1 infection to limit type I IFN production. *J Clin Invest* **131** (2021).

1014

1015 69. Yang, K. *et al.* Metabolic signaling directs the reciprocal lineage decisions of alphabeta and  
1016 gammadelta T cells. *Sci Immunol* **3** (2018).

1017

1018 70. Sanson, K.R. *et al.* Optimized libraries for CRISPR-Cas9 genetic screens with multiple modalities.  
1019 *Nat Commun* **9**, 5416 (2018).

1020

1021

## Supplementary Files

This is a list of supplementary files associated with this preprint. Click to download.

- [SupplementNComm.pdf](#)